Received: 2 February 2022 | Revised: 26 August 2022 | Accepted: 1 October 2022

DOI: 10.1111/bre.12725

Basin Research | IAS EAGE | WILEY

RESEARCH ARTICLE

Shaking and splashing—A case study of far-field effects of the Mjølnir asteroid impact on depositional environments in the Barents Sea

Rikke Bruhn[1,2] | **Jenő Nagy**[1] | **Morten Smelror**[3] | **Henning Dypvik**[1,4] | **Sylfest Glimsdal**[5] | **Richard Pegrum**[2] | **Carlo Cavalli**[2]

[1]Department of Geosciences, University of Oslo, Oslo, Norway

[2]Dong E&P Norway AS, now PGNIG Upstream Norway AS, Stavanger, Norway

[3]Geological Survey of Norway, Trondheim, Norway

[4]Department of Technology Systems, University of Oslo, Oslo, Norway

[5]Norwegian Geotechnical Institute, Oslo, Norway

Correspondence
Rikke Bruhn, Department of Geosciences, University of Oslo, P.O. Box 1047, NO-0316 Oslo, Norway.
Email: rikke.bruhn@geo.uio.no

Abstract

The Mjølnir impact crater in the Norwegian Barents Sea features among the 20 largest impact craters listed in the Earth Impact Database. The impact is dated to 142 ± 2.6 Ma, corresponding closely to the Jurassic/Cretaceous boundary in the Boreal stratigraphy. Multidisciplinary studies carried out over the last three decades have suggested that the up to 40 km wide crater was created by a 1–3 km diameter impactor colliding with a shallow epicontinental sea, causing regional havoc and a regional ecological crisis that followed in its wake. Only minor evidence for the consequences of the impact for the surrounding depositional basins has been documented so far. This study describes a large submarine slump penetrated by hydrocarbon exploration well 7121/9-1, located in the southern Hammerfest Basin and approximately 350 km away from the impact site. The slump is dated by a black shale drape, which contains characteristic impact-related biotic assemblages and potential ejecta material. This precise dating enables us to associate the slump with large-scale fault movements and footwall collapse along the basin-bounding Troms-Finnmark Fault Complex, which we conclude were caused by shock waves from the Mjølnir impact and the passage of associated tsunami trains. The draping black shale is interpreted to represent significant reworking of material from the contemporary seabed by tsunamis and currents set up by the impact.

KEYWORDS

asteroid impact, fault movement, impact-related deposits, submarine slump

1 | INTRODUCTION

The Mjølnir impact crater, buried on the Bjarmeland Platform in the central Barents Sea at 73°48′N/29°40′ E, was first recognized in commercial 2D seismic data (Gudlaugsson, 1993) and accepted into the Earth Impact Database in 1996 following recovery of diagnostic impact-derived material close to the impact site

(Figure 1) (Dypvik et al., 1996, 2004). With a maximum apparent diameter of 40 km, it is likely among the 20 largest impact-structures currently recognized on Earth.

The Mjølnir impact structure and its immediate surroundings are penetrated by two dedicated research boreholes: 7329/03-U-01 and 7430/10-U-01. In addition, the Bjarmeland Platform and central-western Barents Sea in general is densely covered by commercial seismic data and hydrocarbon exploration wells. The data coverage and accessibility make the Barents Sea an ideal marine shelf setting for analysing both near and remote impact consequences.

As a result, Mjølnir is one of the most well-studied shallow marine impact sites, comparable to the much larger Late Eocene Chesapeake Bay and Cretaceous-Paleogene Chicxulub craters (Dypvik et al., 2018, Gohn et al., 2009, Gulick et al., 2013, Hildebrand et al., 1995, Powars et al., 1993, Schulte et al., 2010).

In the present paper, we describe a large submarine slump deposit informally referred to as the Zapffe unit, based on seismic interpretations and observations from hydrocarbon exploration well 7121/9-1 Zapffe (Figure 1). The Zapffe unit has not previously been described nor has its formation been associated with the Mjølnir impact. We consider our study case to be the first well-documented example of a plausible Mjølnir-related deposit located away from the impact site itself. Our observations suggest that the impact triggered widespread tsunami-related seabed erosion in the Hammerfest Basin and potentially also large-scale activation of major faults several hundred kilometres away from the impact site. We additionally discuss some relations between impact forcing and basin topography that may aid in future recognition of impact-related deposits in the Barents Sea and elsewhere.

Highlights

- We accurately date a slump in the Barents Sea to coincide with the Mjølner asteroid impact using biostratigraphy.
- This is the first record of sedimentary effects of the impact away from the crater itself.
- We imply that the impact triggered large-scale faulting and creation of submarine cliffs at least 60 m high.
- We suggest that large volumes of mud were eroded from the seabed by waves and currents set up by the Mjølnir tsunami.
- We document the immediate post-impact ecological crisis caused by tsunami backwash of nutrients to the marine realm.

2 | REGIONAL SETTING OF THE LATE JURASSIC—EARLY CRETACEOUS IN THE SOUTHWESTERN BARENTS SEA

The study area is located in the southern Hammerfest Basin, close to the Troms-Finnmark Fault Complex (Gabrielsen, 1984) and approximately 350 km from the Mjølnir impact site (Figure 1). The Hammerfest Basin region formed part of the slowly subsiding Barents Sea epicontinental basin throughout the Mesozoic. It came to its present shape during a period of Late Jurassic to Early Cretaceous extension associated with the evolution of the North Atlantic rift system (Faleide et al., 2015; Gabrielsen, 1984; Gabrielsen et al., 1990).

2.1 | Stratigraphy and depositional environments

The latest Jurassic and earliest Cretaceous stratigraphy of the area is displayed by the marine Fuglen, Hekkingen and Knurr formations (Mørk et al., 1999; Worsley et al., 1988) (Figure 2). The Fuglen Formation is a relatively thin (m to tens of m) retrograding siltstone succession that marks the Bathonian—Oxfordian marine transgression across Early and Mid-Jurassic coastal plain and nearshore environments (Figure 2).

Widespread deposition of Hekkingen Formation organic-rich marine clays followed, with stable anoxic to hypoxic 'Kimmeridge Clay sea' conditions persisting throughout the remainder of the Late Jurassic and in places into the earliest Cretaceous (Figure 2) (Georgiev et al., 2017; Langrock & Stein, 2004; Marin et al., 2021; Smelror & Dypvik, 2006). None of the wells in the southern Hammerfest Basin has penetrated significant sandstones in the Hekkingen Formation, suggesting that the latest Jurassic coastline was located on the Finnmark Platform, south of the present-day basin bounding Troms-Finnmark Fault Complex. The presence of numerous minor Hekkingen Formation depocentres along the Troms-Finnmark Fault Complex indicate onset of extension along segments of this basement-cored, Palaeozoic fault zone from the Kimmeridgian, particularly in the western part of our study area (Figure 3) and in the Alke and Goliat areas at the western and eastern limits of the study area, cf. Mulrooney et al. (2017) and Muzaffar (2018).

The Knurr Formation consists of marine calcareous mudstones deposited under oxic, open marine conditions in the Ryazanian–Barremian (Worsley et al., 1988; Mørk et al., 1999). The formation contains thick, wedge-shaped

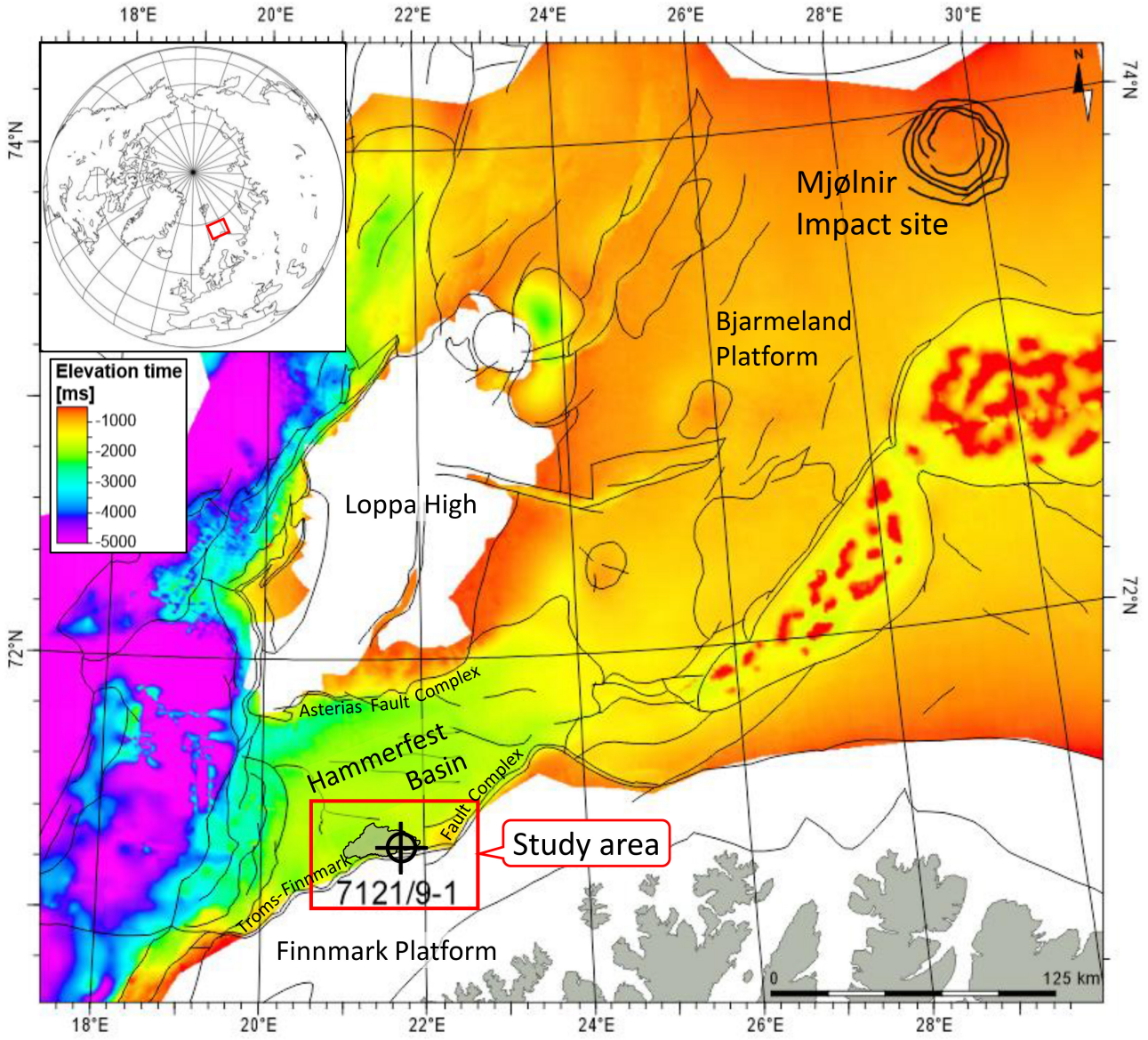

FIGURE 1 Location map of the study area and well 7121/9-1, showing the time structure to top Hekkingen Formation. Present-day Norway in grey shading. Major faults (black lines) and structural elements are sourced from NPD factmaps (https://factmaps.npd.no/factmaps/3_0/). The Mjølnir impact site is located approximately 350 km north-northeast of the study area. The study area for this paper is marked with red, with the lateral extent of the Zapffe unit shaded in grey.

prisms and mounds of marine density flow deposits along major fault scarps in the Troms-Finnmark Fault Complex (Figure 3), and along the Asterias Fault Complex bounding the southern Loppa High (Figure 1). These document the presence of significant topography and bathymetry controlled by normal faulting during the Early Cretaceous (Marin et al., 2018).

2.2 | The Mjølnir impact and its perturbation of depositional environments

The Mjølnir impact has been biostratigraphically dated to 142 ± 2.6 Ma (Smelror et al., 2001) and 141.9 ± 2.7 Ma by Re-Os chronology (Hannah et al., 2020). These ages approximate the Boreal Volgian–Ryazanian boundary and are within the Early Berriasian on the GSA Geological Time Scale v.5 (Smelror et al., 2001; Smelror & Dypvik, 2006). Within the accuracy of the available biostratigraphy from hydrocarbon wells in the Hammerfest Basin, this time falls within the uppermost part of the Hekkingen formation or at the Hekkingen—Knurr transition (Worsley et al., 1988; Marin et al., 2021, Mørk et al., 1999, Smelror et al., 2001, Smelror & Dypvik, 2006).

Tsikalas et al. (1998) and Shuvalov et al. (2002) concluded an impactor size of 1–3 km in diameter based on the size of the impact crater and assumptions of velocity

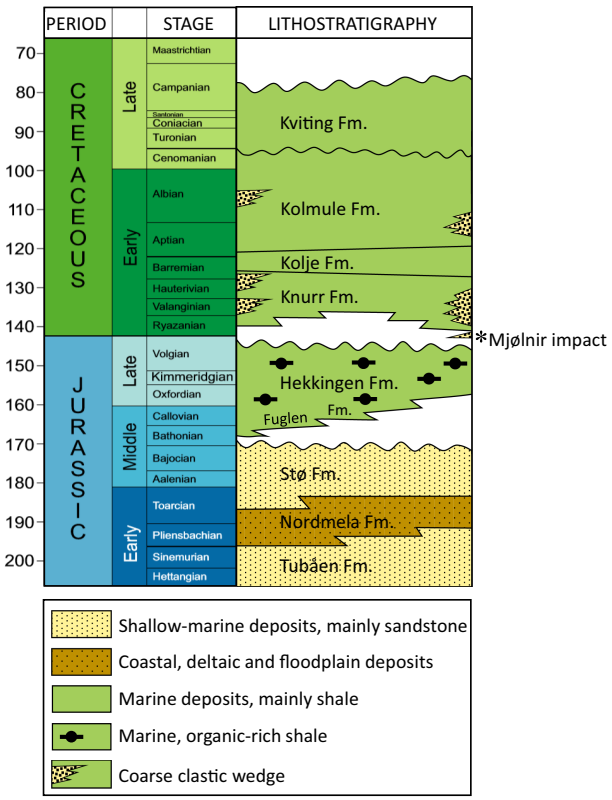

FIGURE 2 Lithostratigraphy of the Jurassic and Early Cretaceous in the Hammerfest Basin. Nomenclature from Worsley et al. (1988) and Mørk et al. (1999). Age of Cretaceous clastic wedges in the Hammerfest Basin from Marin et al. (2018).

and angle of trajectory. They calculated that the impact released a maximum energy on the order of 1.3×10^{22} J, vaporized or ejected 180–230 km^3 of rock mass and created a deep and complex crater (Glimsdal et al., 2007; Morgan et al., 2016; Shuvalov et al., 2002).

The far field propagation of the impact shock waves from the Mjølnir earthquake has, to our knowledge, not been modelled and are not well understood. Rokoengen et al. (2005) attributed fault patterns in marine mudstones offshore mid-Norway to the impact earthquake, and thus suggested the presence of tectonic effects 2000 km away from the impact site. Recently e.g., Güldemeister and Wünnemann (2017) has demonstrated the effects of target properties such as lithology, porosity, and water content on seismic magnitude, which can be predicted using numerical modelling. So far nothing of this nature has been published for the Mjølnir case.

The impact-generated tsunami has been modelled by Shuvalov et al. (2002), and Glimsdal et al. (2007, 2010). The latter modelled an initial several hundred-metre-high wall of water, which broke into trains of waves with a height of 200 m high at a distance of 160 km from the impact site, 20 m high at a distance of 500 km and 5 m at a distance of 2000 km. Wave heights of Glimsdal et al. (2007) were modelled during deep-water propagation and expected to be amplified during shoaling. Along the coasts of North Norway and North Greenland, the bores likely broke at water depths of 200–300 m (Glimsdal et al., 2007), thereby dissipating huge amounts of energy at the seabed and potentially re-suspending large volumes of sediment. Tsunami-related deposits in the Hammerfest Basin, close to our study area, may have been observed although not identified as such by Marin et al. (2021). Attempts to identify the tsunami imprint in the nearshore sedimentary successions of North Greenland have so far proven unsuccessful (Dypvik et al., 1998).

Vast areas of mainland Norway were inundated by the tsunami, and the backflow brought large quantities of fresh water and nutrients into the marine realm, leading to an abrupt bloom of characteristic assemblages of freshwater algae and opportunistic prasinophyte species in the immediate post-impact aftermath (Bremer et al., 2004; Smelror et al., 2001; Smelror & Dypvik, 2005, 2006). These biotic assemblages are often found in combination with fallout material and soot and form a layer which is a unique time-marker for the impact. This layer has been identified in boreholes close to the crater, in several hydrocarbon exploration wells across the Barents Sea, in the Myklegardfjellet Bed of the Agardhfjellet Formation on Svalbard and in Northern Siberia (Dypvik & Attrep, 1999; Dypvik & Ferrell, 1998; Smelror & Dypvik, 2005; Zakharov et al., 1993).

3 | OUR OBSERVATIONS FROM THE ZAPFFE UNIT AND WELL 7121/9-1

The focus for our study is a depositional unit, here informally named Zapffe, which locally separates the seismically defined Hekkingen and Knurr formations at a burial depth of around 1800 ms two-way travel time (TWT) or approximately 2000 m in the southernmost Hammerfest Basin (Figures 1 and 4). This unit has not previously been described or dated. The key locality of the Zapffe unit is the 7121/9-1 exploration well, drilled by DONG E&P Norge AS in 2011, which targeted the unit as a hydrocarbon prospect (Figures 1 and 4).

3.1 | Seismic expression of the Zapffe unit

The Zapffe unit was mapped on the DG0901 PSDM 3D seismic survey. The survey was acquired by Fugro in 2009 using an airgun source and a 4.5 km geophone streamer array. It was pre-processed by CGGVeritas using

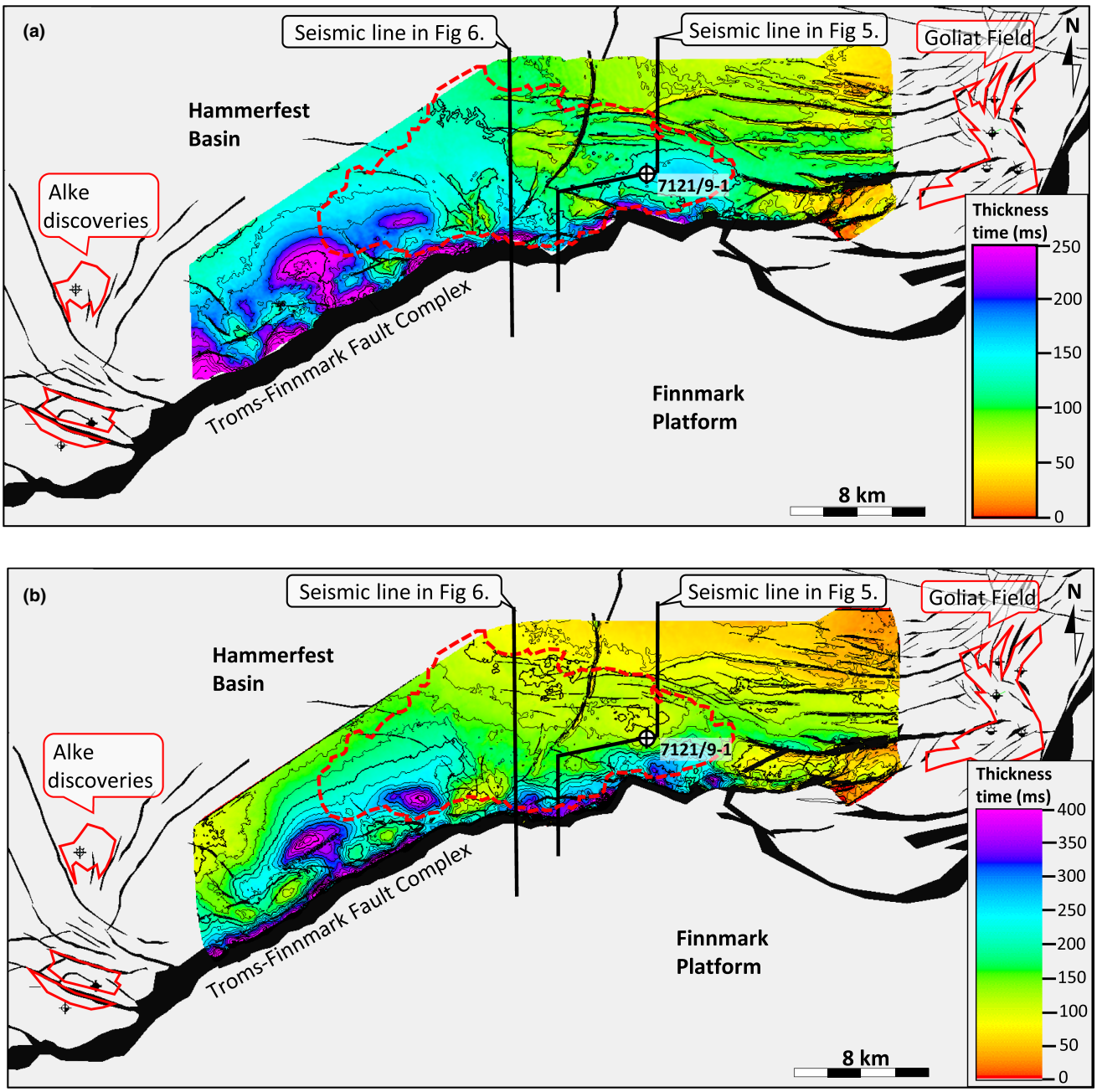

FIGURE 3 TWT isopach maps of the Hekkingen and Knurr formations. (a) Hekkingen Formation. (b) Knurr Formation. Both maps are created as vertical thickness maps and therefore overestimate thickness of a formation in areas with steeply dipping strata, in particular close to the main faults in the Troms-Finnmark fault complex. The outline of the Zapffe unit is marked in dashed red line in both maps.

a standard workflow, time-migrated and subsequently depth-migrated (Gomez et al., 2012). The resulting datasets (PSTM & PSDM, full and angle stacks) have a 25 × 25 m grid spacing, normal polarity (increase of acoustic impedance = positive reflection coefficient displayed as a positive number), and a dominating frequency at target depth of about 40 Hz.

The Zapffe unit is a continuous feature along approximately 25 km of the Troms-Finnmark Fault Complex (Figures 4–6). It thickens rapidly away from the fault zone and then gradually tapers into a characteristic set of lobes, which extend 6–10 km northward into the Hammerfest Basin (Figure 4). In N-S cross sections, the unit is broadly lenticular with a thickness of up to about 150 m (Figures 5 and 6).

The base of the unit was picked in a laterally continuous acoustically soft reflector (marking a downward decrease in acoustic impedance) at the top of the concordant and parallel stratified Hekkingen Formation shale package (Figures 5 and 6). The Hekkingen Formation is truncated locally below the central parts of the Zapffe unit (Figure 6) and generally across local intra-basinal highs

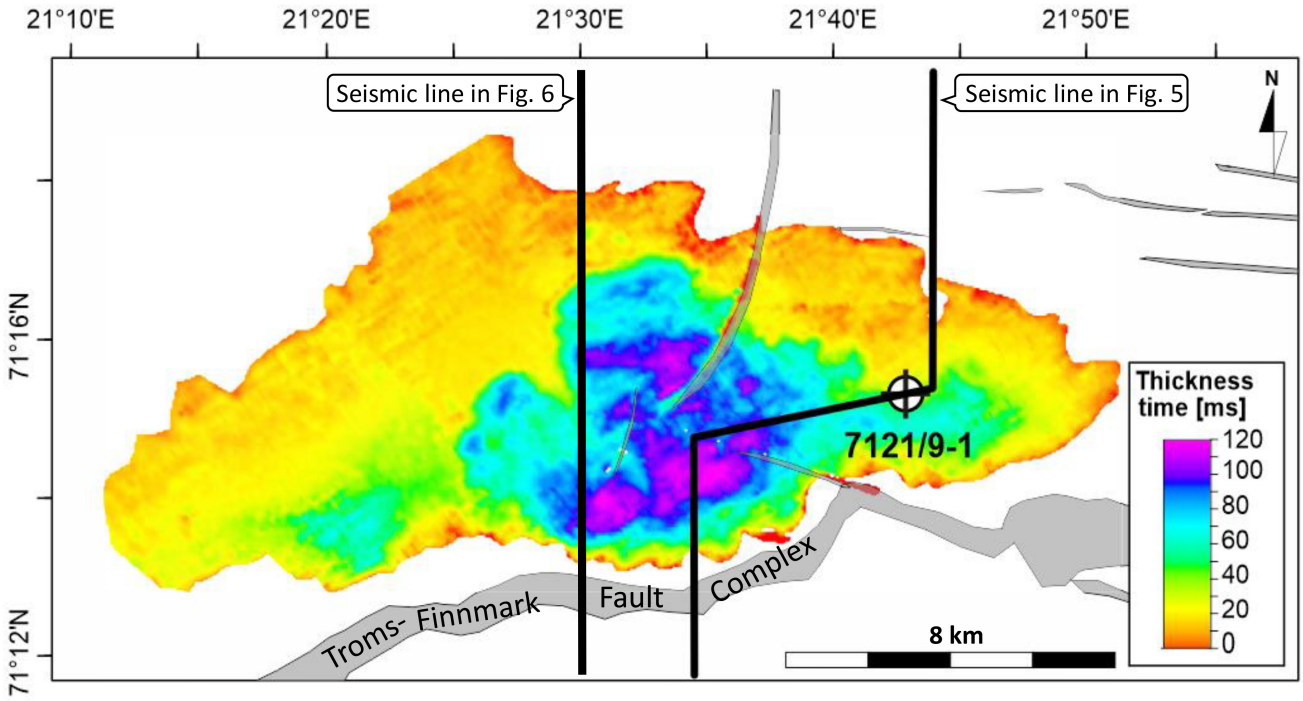

FIGURE 4 Time thickness map of the Zapffe unit and location in relation to the Troms-Finnmark Fault Complex and well 7121/9-1.

in the Hammerfest Basin (Figure 5) as also documented by Marin et al. (2021). The seismic top Zapffe surface was picked as a laterally consistent, acoustically soft reflector (Figures 5 and 6). This has an uneven relief of up to 60 ms TWT (approximately 100 m), most distinctly associated with localized thickness maxima in the frontal part of the middle lobe (Figures 4 and 6). Internal reflectivity patterns in the unit are transparent to chaotic or shingled with south-dipping imbricated reflectors (Figure 6). The localized thickness maxima in the frontal part of the unit are associated with areas of internally parallel strata, in places with enhanced reflectivity at top and base compared to neighbouring parts of the Zapffe unit (Figure 6).

The Zapffe unit is overlain by the Knurr Formation, which has a strong wedge-shaped geometry and thickens towards the Troms-Finnmark Fault Complex (Figures 5 and 6).

3.2 | Lithostratigraphy in well 7121/9-1

The 7121/9-1 well penetrates the north-eastern part of the Zapffe unit in a location where it is relatively thin (50 m) compared to the central parts (150 m) (Figure 5). An excellent well tie to the DG0901 PSDM 3D seismic survey was achieved through calibration of the sonic log to a vertical seismic profile (VSP) survey, combined with density modelling above log coverage from offset wells (Figure 5). The well was not cored, but a comprehensive wireline log suite was acquired, and several sidewall cores (SWC) were recovered from the Hekkingen Formation, Zapffe unit and basal part of the Knurr Formation (Figure 7).

The Hekkingen Formation is more than 200 m thick in the well and consists entirely of black organic-rich shales with groups of limestone/dolomite stringers, responsible for the observed internal seismic reflectivity at the well location (Figures 5 and 7). A sidewall core (SWC) at 2090 m measured depth below the rotary table (MD) shows that the shale is horizontally laminated with no bioturbation.

The top Hekkingen Formation/base Zapffe unit at 2077 m MD, as it was interpreted prior to drilling well 7121/9-1, is marked with a turquoise line in Figure 7. The seismic reflector turned out to correspond to an acoustic impedance decrease at the base of a tightly calcite-cemented siltstone interval in 2070 to 2075 m MD in the well. The cemented interval is similar to dolomite stringer groups in the upper Hekkingen Formation deeper in the well and may indeed represent the uppermost Hekkingen Formation. It is therefore possible that the depositional base of the Zapffe unit could be located somewhat above the seismically defined base. We shall however keep the seismically defined 2077 m MD as the base of the Zapffe unit because it is difficult to define an alternative, shallower base from available well data, and because the seismically defined base corresponds to a laterally consistent seismic marker and therefore facilitates the correlation between seismic and well observations.

The Zapffe unit (2077–2027 m MD), between the turquoise and green lines in Figure 7, is dominated by mudstone and muddy sandstone, with 1–2 m thick, cleaner

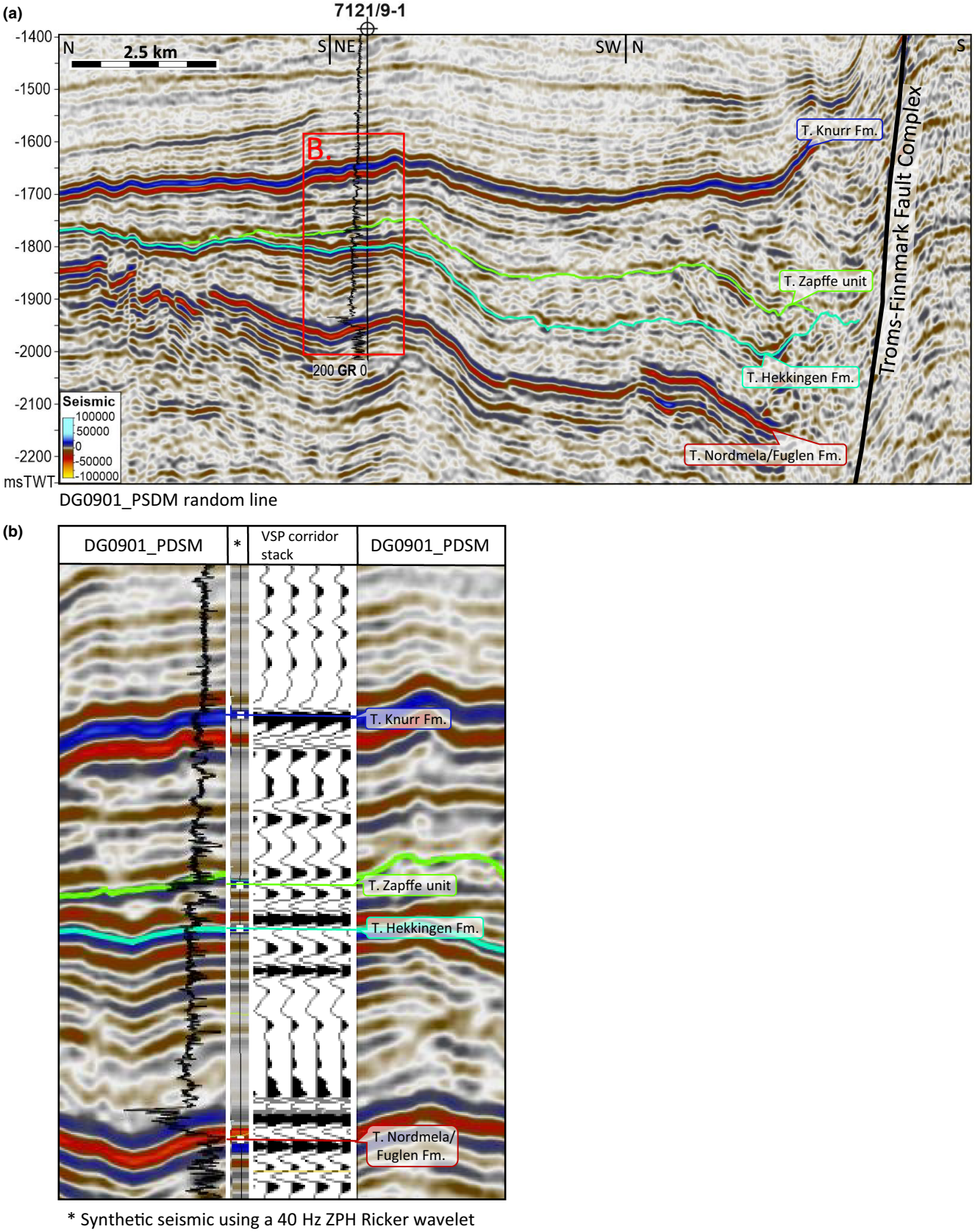

FIGURE 5 (a) Seismic section through the Zapffe unit and well 7121/9-1. Red box marks the section of the well tie shown in (b). Refer to text for further discussion. (b) Seismic to well tie, comparing the seismic immediately around 7121/9-1 with a synthetic seismic created with a 40 Hz ZPH Ricker wavelet, and the VSP corridor stack acquired in 7121/9-1.

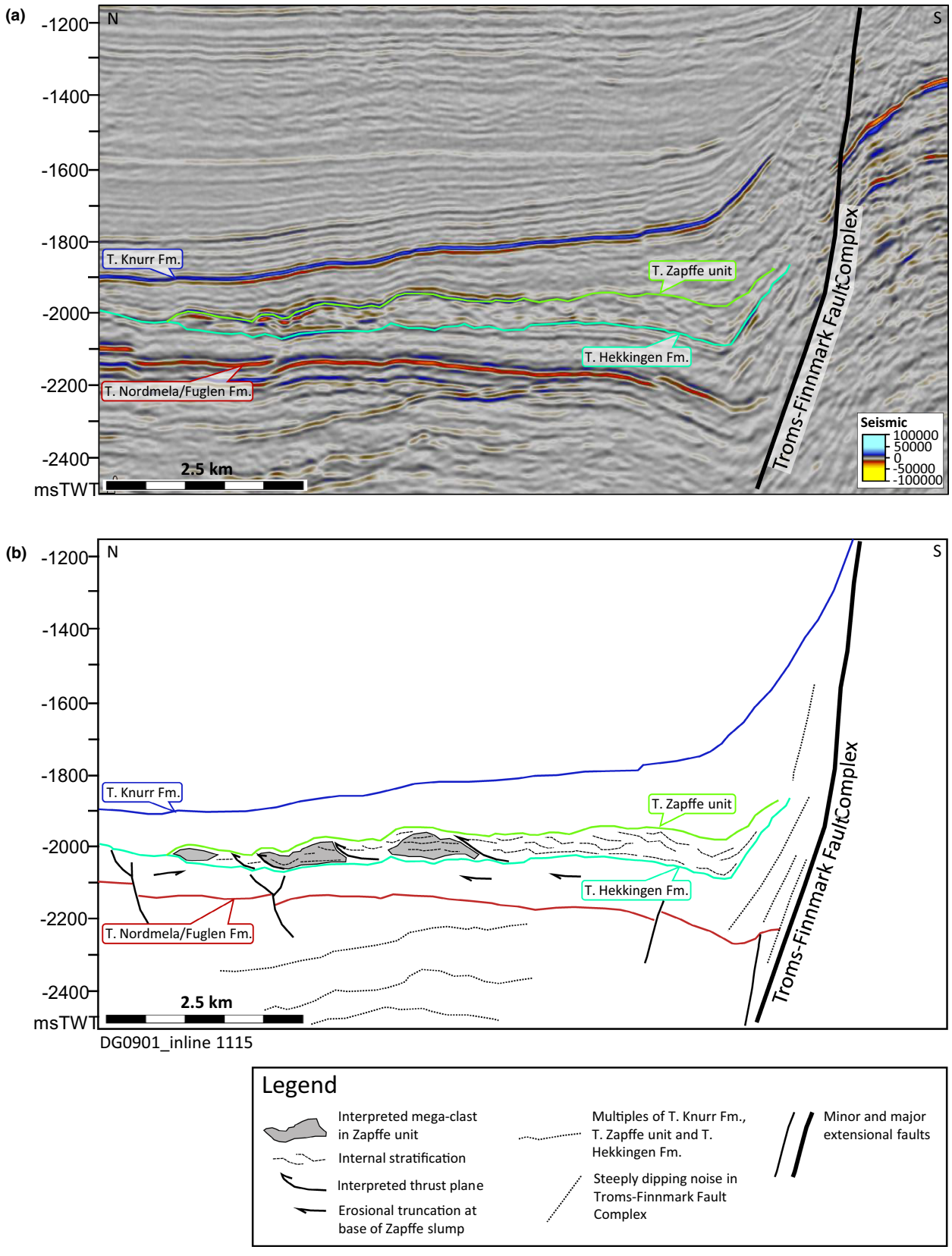

FIGURE 6 Seismic line with seismic architecture interpretation through main part of Zapffe. (a) Seismic line with marking of the main stratigraphic unit boundaries only, and (b) interpretation of seismic line in (a). Reflector geometries internally in the Zapffe unit display chaotic to shingling patterns, and areas of internally parallel reflector patterns in the frontal (northern) part of the unit are interpreted to be megaclasts derived from the fault scarp. Reflector patterns are generally difficult to interpret with confidence close to the fault scarp, probably as a result of real lateral depositional changes, tectonic disturbance and noise in the seismic.

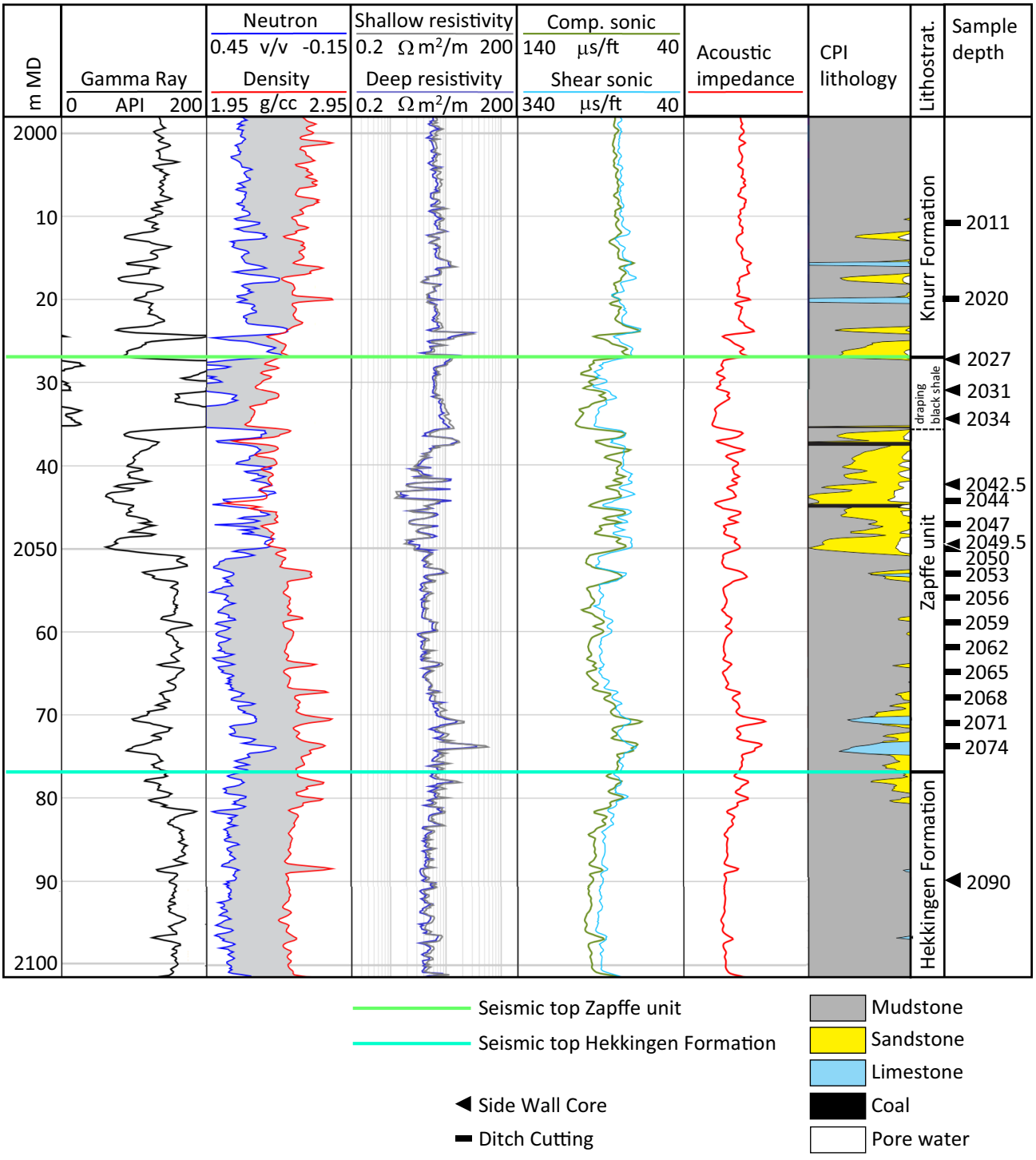

FIGURE 7 7121/9-1 well logs, calculated lithology (CPI) and position of ditch cutting samples and sidewall cores used in lithology description and biostratigraphic analysis; far right column (sample depth). The seismic top Hekkingen Formation and top Zapffe unit are indicated by coloured lines as in Figures 5 and 6.

sandstone intervals and traces of coal (Figure 7). In sidewall cores, the sandstones appear massive or have irregular stratification or banding, and the coal occurs as angular clasts (Figure 8). In the thin section, the sandstone intervals are seen to contain high proportions of orientated shale filaments and amorphous organic material defining a subhorizontal banding (Burfoot & Dunk, 2012) (Figure 8).

A black, horizontally laminated draping shale interval is present in the well from 2027–2036 m MD and represented by two SWC in levels 2031 and 2034 m MD (Figure 7). This interval represents the upper seismic level of the Zapffe unit and was interpreted as the top of a sandstone prior to drilling, based on its acoustically soft signature. The shale interval displays very high gamma ray values (>200 API)

FIGURE 8 Photos and thin section micrographs of sidewall cores in and immediately above the Zapffe unit (see Figure 7), adapted from Burfoot and Dunk (2012). (a) Sidewall core from 2042.5 m MD, consisting of very fine-grained, laminated sandstone with an angular coal clast. Approximately 25% of the clasts are uneven filaments of clay (Hekkingen formation clasts) and amorphous organic material. (b) Sidewall core from 2027 m MD, consisting of very fine-grained, massive or crudely laminated sandstone. The minor content of lithic clasts in this sample (1.7%) consists of highly altered clay clasts or glauconite pellets, and clasts of quartz and feldspar shards set in a fine-grained groundmass that may be altered glass.

and total organic content (TOC) up to 10%; far exceeding values of the immediately underlying shales in the upper Hekkingen formation and only matched by TOC values of the lowermost Hekkingen, located 250–300 m deeper in the well (Nyjordet et al., 2012). The kerogen of the SWC in 2031 and 2034 m MD consists of 80%–88% amorphous material, 10%–15% algae and dinoflagellates, and small amounts of wood and coal (Appendix A). This contrasts with the composition of organic material in the underlying Hekkingen formation, which is generally less amorphous and containing 15%–20% sporomorphs and woody/coaly material (Nyjordet et al., 2012).

The Knurr Formation encountered in 1809–2027 m MD in the well, consists of mudstone with minor thin sandstone beds, particularly in the lower part of the formation (Figure 7). A SWC in 2027 m MD which samples the thin sandstone at the base of the Knurr Formation, contains highly altered clay or possibly glauconite clasts and clasts of fine quartz and feldspar shards set in a very fine light brown groundmass. The brown groundmass was interpreted as potential altered glass by Burfoot and Dunk (2012) (Figure 8).

3.3 | Biostratigraphy in well 7121/9-1

Biostratigraphic sample material from the Late Jurassic and Early Cretaceous of well 7121/9-1 was recently re-analysed for palynomorphs and analysed for the first time for foraminifers with the purpose of age assessments and contribution to environmental interpretations to this paper. Range charts are supplied in Figures 9 and 10, and the plates of the encountered species are supplied in Appendices B and C. There is a general agreement of ages indicated by the well-preserved palynoflora and the foraminiferal distributions.

Samples for palynological analyses were processed following standard palynological preparation methods at the laboratory of CGG Robertson (UK) (Fenton et al., 2012). The palynological semi-quantitative analyses were carried out by transmitted light microscopy and recorded specimens in selected samples covering the Zapffe unit and nearby strata are listed in Figure 9. Nineteen (19) sediment samples were processed in the laboratory for foraminifera analysis, of which 9 from the lower and middle part of the Zapffe unit were productive, while samples from the upper part were barren (Figure 10). The samples were disintegrated according to the tenside method of Nagy (2005) and washed through a sieve-set with mesh diameters of 63, 90, 125 and 500 µm, with the fractions from 90 to 500 µm selected for species identification and counting. The alpha diversity index given in Figure 10 is calculated by $S = a^{*}\ln(1+n/a)$, where S is number of taxa, n is number of individuals and a is the Fisher's alpha (Murray, 2006).

Age	Formation	Depth, m MD	Ditch cuttings / Side Wall cores	*Atopodinium haromense*	*Chalydophorella nyei*	*Circulodinium distinctum*	*Cleistosphaeridium spp.*	*Cribroperidinium spp.*	*Egmontodinium expiratum*	*Endoscrinium anceps*	*Gonyaulacysta cassidata*	*Muderongia tetracantha*	*Oligosphaeridium complex*	*Oligosphaeridium asterigerum*	*Gonuaulacysta dualis*	*Cribroperidinium globatum*	*Dichadogonyaulax sp.*	*Tasmanites spp.*	*Circulodinium brevispinosum*	*Oligosphaeridium diculum*	*Kleithriasphaeridium corrugatum*	*Achomosphaera? neptuni*	*Gochteodinia villosa*
Val.	Knurr	1948.0	DC	x	x	x	x	x	x	x	x	x	x										
Val.	Knurr	1960.0	DC			x	x						x	x	x	x	x						
Val.	Knurr	1972.0	DC			x	x			x			x					x	x	x	x		
L.R.	Knurr	1984.0	DC		x	x	x													x	x		
L. Volg. - E. Ryazan.	Zapffe'	1993.0	DC			x	x															x	x
L. Volg. - E. Ryazan.	Zapffe'	2011.0	DC			x	x												x	x	x	x	x
L. Volg. - E. Ryazan.	Zapffe'	2020.0	DC	x			C	x							x					x			C
L. Volg. - E. Ryazan.	Zapffe'	2031.0	SW															x					
L. Volg. - E. Ryazan.	Hekkingen	2034.0	SW					x															
L. Volg. - E. Ryazan.	Hekkingen	2047.0	DC				x																
L. Volg. - E. Ryazan.	Hekkingen	2056.0	DC					x															
L. Volg. - E. Ryazan.	Hekkingen	2074.0	DC					x															x
L. Volg. - E. Ryazan.	Hekkingen	2090.0	SW	x			x	x															x
E. - M. Volgian	Hekkingen	2107.0	DC				x	x															
E. - M. Volgian	Hekkingen	2119.0	DC																				
E. - M. Volgian	Hekkingen	2128.0	DC	x			x								x								
E. - M. Volgian	Hekkingen	2155.0	SW	x																			
E. - M. Volgian	Hekkingen	2164.0	DC					x															
E. - M. Volgian	Hekkingen	2173.0	DC					x															
E. - M. Volgian	Hekkingen	2191.0	DC					x								x							
E. - M. Volgian	Hekkingen	2198.0	SW				x	x								x							
E. - M. Volgian	Hekkingen	2205.0	SW	x			x								x								
E. - M. Volgian	Hekkingen	2227.0	DC					x								x		x					
E. - M. Volgian	Hekkingen	2240.0	SW																				

Depth, m MD	*Gonyaulacysta fastigiata*	*Hystrichosphaeridium pulchrum*	*Sirmiodinium grossii*	*Tubotuberelle apatela*	*Circulodinium compacta*	*Egmontodinium toryna*	*Gonyaulacysta jurassica*	*Kleithrisphaeridium sp.*	*Lagenorhytis delicantula*	*Leptodinium subtile*	*Perisseiasphaeridium pannosum*	*Rhynchodiniopsis cladophora*	*Scriniodinium crystallinum*	*Cassiculosphaerdia magna*	*Escharisphaeridia pocockii*	*Oligosphaeridium patulum*	*Paragonyaulacysta borealis*	*Subtilisphaera? Inaffecta*	*Systematophora daveyi*	*Tubotuberella dangeardii*
1948.0																				
1960.0																				
1972.0																				
1984.0																				
1993.0	x	x	x	x																
2011.0	x	x	x	x	x	x	x	x	x	x	x	x	x							
2020.0			x	x							x			x	x	x	x	x	C	x
2031.0																				
2034.0																				
2047.0		x	x													x				
2056.0																				
2074.0		x	x	x								x								
2090.0	x	x	x	x							x				x	x				
2107.0		x	x												x	x				
2119.0		x	x	x							x			x			x			x
2128.0		x	x	x							x									
2155.0			x	x								x					x			
2164.0			x															x		
2173.0			x	x								x								
2191.0			x												x			x		
2198.0				x													x			
2205.0			x							x							x			
2227.0		x												x						
2240.0			x												x	x	x			

Depth, m MD	*Botryococcus spp.*	*Leiosphaeridia spp.*	*Cyclopsiella spp.*	*Scriniodinium inritibile*	*Gonyaulacysta jurassica*	*Proxilosphaeridium spp.*	*Rhynchodiniopsis martonense*	*Leptodinium subtile*	*Systematophora areolata*	*Chlamydophorella cf. ectotabulata*	*Sentusidinium spp.*	*Dingodinium minutum*	*Leptodinium antigonium*	*Hytrichosphaeridia orbifera*	*Glossodinium dimorphum*	*Lithodinia spp.*	*Gen et sp. Indet*	*Gen et sp. Indet 2*	*Pareodinia ceratophora*	*Senoniasphaera jurassica*
1948.0																				
1960.0																				
1972.0																				
1984.0																				
1993.0																				
2011.0																				
2020.0																				
2031.0	x	x																		
2034.0			x	x	x															
2047.0						x	x													
2056.0								x	x											
2074.0									x	x	x									
2090.0	x	x							x		x	x								
2107.0										x			x							
2119.0								x		x			x							
2128.0				x				x	x			x		x						
2155.0				x		x	x				x				x	x				
2164.0		x		x									x				C			
2173.0		x								x			x					x	x	x
2191.0		x							x									x		
2198.0		x									x							x		
2205.0																				
2227.0											x								x	
2240.0				x				x				x						x		x

FIGURE 9 Palynostratigraphic range chart of marine (dinoflagellate cysts and acritarchs) and freshwater algae (*Botryococcus* sp.) recovered in the Volgian-Valanginian strata in well 7121/9-1. X = marks recorded species in each sample; C = common occurrence of a species.

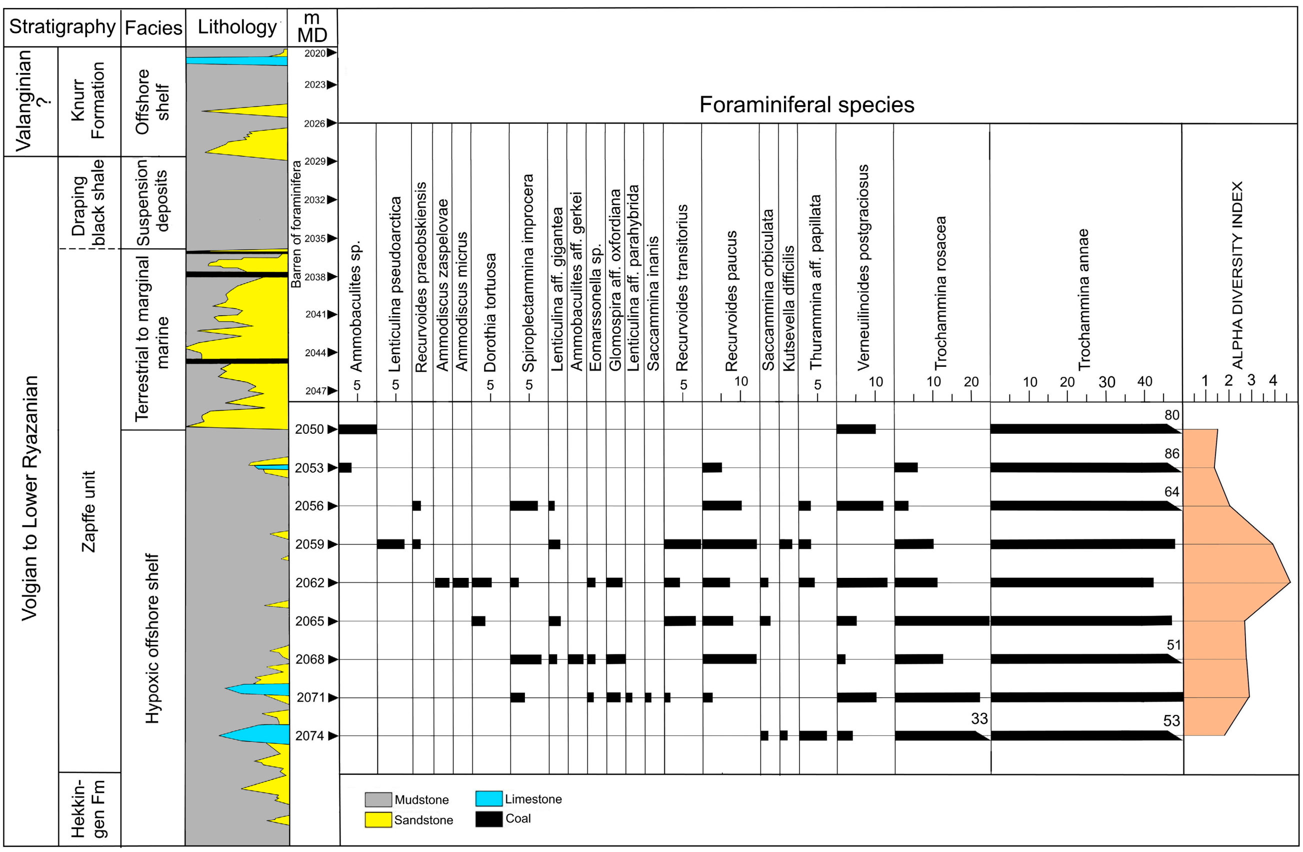

FIGURE 10 Range chart of foraminiferal species in percent covering the lower and middle part of the Zapffe unit in well 7121/9-1. Absolute values of each species are marked for each sample depths by the black bars, and large values are specified in percent next to the bars.

Our analysis shows that the entire Hekkingen Formation is impoverished in microfauna with few age-diagnostic species, in trend with regional characteristics of this depositional unit. However, the occurrence of *Gochteodinia villosa* at 2090 m (SWC) immediately below the Zapffe unit suggests an age not older than Late Volgian (*Oppressus* ammonite zone) for the upper part of the Hekkingen Formation (Poulsen & Riding, 2003; Riding & Thomas, 1992) (Figure 9).

Among palynomorphs in the Zapffe unit, the regular to common occurrence of *Gochteodinia villosa* is evidence of an age within the Late Volgian to Early Ryazanian time interval (Figure 9). Noteworthy, the sample at 2047 m MD contains the dinoflagellate *Rhynchodiniospsis martonense* indicating the middle Early Volgian (Fenton et al., 2012). However, given the younger age from the underlying Hekkingen Formation, this is likely to be reworked. This interpretation is supported by the recovery of *Gonyaulacysta jurassic* in the SWC at 2034 m MD, a species with a last occurrence datum in the Early Volgian. Additional evidence of reworking from underlying Volgian deposits are *Subtilisphaera? inaffecta* at 2164 m MD, a species typically not found in strata younger than Early/mid Volgian (Riding & Thomas, 1992), and the common occurrence of Dinoflagellate sp. indet 2 reported by Bjærke (1980) in his zone 3 on Spitsbergen. Bjærke (1980) suggested an Early Volgian age, possibly extending into the latest Kimmeridgian, for zone 3. However, as zone 3 was reported to occur within the '*dorsoplanus*' zone by Bjærke (1980), this informal dinocyst zone is rather assigned to the middle Volgian. The presence of *Glossodinium dimorphum* at 2155 m MD supports the mentioned evidence of reworking from middle Volgian or older upper Jurassic strata into the Zapffe unit.

The draping black shale at the top of the Zapffe unit is highly impoverished with no age-diagnostic species, but it contains a significant influx of *Botryococcus* spp and the prasinophyte algae *Leiosphaeridia* and *Tasmanites* (Figure 9, Appendix A). The presence of rare Kimmeridgian and older forms in the SWC in 2034 m MD points to an inclusion of reworked older parts of the Hekkingen Formation in this interval (Fenton et al., 2012).

Foraminiferal assemblages of the shale-prone lower and middle Zapffe unit (Figure 10) are of Boreal nature and show close similarities to faunas of this realm recorded by Basov et al. (1989), Bulynnikova et al. (1990), Azbel and Grigyalis (1991), and Nagy and Basov (1998). By using data from these publications, the most age significant species of the Zapffe unit (Figure 10) have following stratigraphic ranges: *Recurvoides transitorius*, Late Volgian to Early Ryazanian; *Recurvoides praeobskiensis*, Late Volgian to Early Ryazanian; *Recurvoides paucus*, Late Ryazanian to Early Valanginian; *Ammodiscus zaspelovae*, Volgian; *Lenticulina pseudoarctica*, Ryazanian to Early Valanginian; *Dorothia tortuosa*, Volgian to Ryazanian; *Trochammina annae*, Late Kimmeridgian to Volgian; *Trochammina rosacea*, Volgian; *Verneuilinoides postgraciosus*, Kimmeridgian to Early Volgian.

The stratigraphic ranges mentioned above show that the two short-ranging species with distinct morphology, *Recurvoides transitorius* and *R. praeobskiensis* are restricted to the Late Volgian to Early Ryazanian interval. Furthermore, the ranges of four species are within the Volgian to Ryazanian interval and the partial ranges of three species are in the Volgian or Ryazanian. It suggests that the lower and middle shale intervals of the Zapffe unit belong to the Volgian to Ryazanian Stage, and within this probably to Late Volgian to Early Ryazan Substage (Figure 10).

Samples from the sandstone interval in the upper Zapffe and the draping black shale are barren of foraminifera.

The lower part of the Knurr Formation is likely to be of Late Ryazanian age, as suggested by the presence of the dinoflagellate *Perisseiasphaeridium insolitum* (Fenton et al., 2012) and occurrence of *Circulodinium compactum* and *Egmontodinium torynum* in a cuttings sample from 2011 m MD, that is, some 16 m above the black shale draping the Zapffe unit (Figure 9). The cuttings sample at 1984 m, contains *Kleithriasphaeridium corrugatum* and *Oligosphaeridium diculum* suggesting a Late Ryazanian age (Costa & Davey, 1992). The dinoflagellate cysts *Muderongia tetracantha* recovered at 1948 m and *Oligosphaeridium complex* found between 1948 and 1972 m in the Knurr Formation points to an age not older than Valanginian.

The biostratigraphic samples through the Knurr Formation indicate abundant recycling of Triassic and Jurassic sediments with Triassic recycling becoming more conspicuous in the upper part. Presence of *Scriniodinium crystallinum*, *Stephanelytron scarburghense* and *Gonyaulacysta jurassica* between 2011 and 2020 m suggest the recycling of Kimmeridgian Hekkingen and Fuglen formations, while rare *Nannoceratopsis ambonis* and *N. senex* between 2011 and 2031 m (SWC) indicate the inclusion of Early Bajocian–Late Pliensbachian strata into the lower part of the Knurr Formation (Fenton et al., 2012).

4 | INTERPRETATION OF DEPOSITIONAL ENVIRONMENTS

4.1 | Hekkingen Formation

The Hekkingen Formation in the studied part of well 7121/9-1 represent an offshore marine environment with oxygen depleted bottom conditions as is common across the Barents Sea (cf. Langrock & Stein, 2004; Mørk et al., 1999; Worsley et al., 1988).

Regional thickness trends of the Hekkingen Formation indicate creation of some syndepositional accommodation space locally along segments of the Troms-Finnmark Fault Complex, particularly in the western part of the study area (Figure 3), and in the Goliat field as described by Mulrooney et al. (2017) and Alke discoveries, as described by Muzaffar (2018). However, little syndepositional fault growth is evident in the area immediately up-dip (south) of the 7121/9-1 well site, which appear to be a relay zone between two original NE–SW trending segments of the Troms-Finnmark Fault Complex (Figures 3a, 5, and 6). The observation is, however, somewhat hampered by the lack of preservation of the Upper Jurassic succession in the footwall of the Troms-Finnmark Fault Complex in the area. We interpret that the individual segments of the Troms-Finnmark Fault Complex were soft linked only at this time, and that the fault segment up-dip of the Zapffe unit had not yet propagated to surface in the Kimmeridgian to middle Volgian. This, along with the absence of observed soft sediment deformation in the Hekkingen Formation in well 7121/9-1 indicates that the fault complex was represented by a gentle monocline up-dip from the well.

4.2 | Zapffe unit and draping black shale

The foraminiferal assemblages from the lower part of the Zapffe unit are almost entirely agglutinated, with a reduced infaunal component and low species diversity (alpha diversity index range 1.4–4.6) (Figure 10). There is a strong dominance of the epifaunal genus *Trochammina* in the samples, of which the most abundant species, *Trochammina annae* is particularly significant by its reduced test size and high frequency average 58% (range 42%–86%). It is generally assumed that *Trochammina* and especially its small-sized representatives reflect oxygen depletion (Nagy et al., 2010; Reolid et al., 2014). A common prerequisite for bottom water hypoxia is a salinity-stratified water column, suggesting that the mudstones in the lower part of the Zapffe unit was originally deposited in a distal prodelta setting.

We interpret the Zapffe unit to represent the onset of density flow deposits associated with development of a major, fault-controlled depositional slope in the study area. This is based on its location along the Troms-Finnmark Fault Complex, its seismic morphology and the lithology as recorded in well 7121/9-1. The frontal thickness anomalies likely represent large 'outrunner' clasts with preserved internal stratigraphy, while the additional imbricated stratification may represent push ridges and compressional slide planes (Figures 4 and 6). Presence of irregular banding defined by soft mudstone clasts in the sidewall cores of well 7121/9-1 supports a cohesive flow behaviour (Figure 8). The very high overall shale content in the slump, at least at the well location, and presence of (likely redeposited) Volgian microfossils suggests that most of the slumped mass is largely reworked Hekkingen Formation. The sandstones and coals in the upper part of the slump (Figures 7 and 8) are potentially reworked from the Early–Mid Jurassic succession. The presence of coal clasts and absence of foraminifera in the sand-rich samples suggest deposition in a freshwater or strongly brackish environment. In 7121/9-1, these lithologies occur in abundance in the Nordmela and Tubåen formations (Figure 2), located several hundred meters deeper in the well. The sandstone in the slump is the first significant coarse clastic influx to the area since the Oxfordian and indicates the onset of erosion of Early and Middle Jurassic lithologies exposed in an emergent fault scarp up-dip of the slump.

The draping black shale defining the seismic top of the Zapffe unit in the 7121/9-1 well is interpreted to be a laterally widespread pelagic drape, based on the continuous character of the top Zapffe seismic marker and the well-defined horizontal lamination of this interval observed in SWC. Absence of foraminifera in the shales might be explained by highly hypoxic or anoxic bottom water conditions, suggested by the high TOC content and strongly increased gamma activity. Severe oxygen depletion primarily excluded foraminifera in the benthic domain, while planktonic palynomorphs remained less or not affected.

4.3 | Knurr Formation

The wedge-shaped geometry of the Knurr Formation overlying the Zapffe unit (Figures 4–6) indicate that subsidence along the at that time fully emergent Troms-Finnmark Fault Complex continued to be a prominent control on deposition through the Early Cretaceous. Presence of increasingly older reworked Jurassic and Triassic fossils upwards through the Knurr Formation fault apron in the 7121/9-1 well, indicates the gradual, continued exhumation and erosion of lithologies on the footwall block. It is possible that the coastline was located along the fault complex during deposition of this formation, as indicated by Marin et al. (2018, their figure 12).

5 | OUR CASE FOR ASSOCIATING THE ZAPFFE UNIT WITH THE MJØLNIR IMPACT

Our combined palynological and foraminiferal evidence indicate that the Zapffe unit must be constrained to the uppermost Volgian–Lower Ryazanian by the presence of Upper Volgian species in the underlying Hekkingen Formation and Upper Ryazanian species in the Knurr

Formation above. Thus, the age of the Zapffe unit closely correlates to that of the Mjølnir impact.

We consider the draping black shale defining the seismic top of the Zapffe unit to be the likely time marker for the impact itself given its high organic content, presence of *Leiosphaeridia, Tasmanites* and juvenile *Botryococcus* spp. (Appendix A; Smelror et al., 2002; Smelror & Dypvik, 2006).

The algal populations in the shale closely resemble the 'smoking gun' assemblages described by Bremer et al. (2004) and Smelror and Dypvik (2005, 2006) from the oldest post-impact deposits close to the Mjølnir crater and in ejecta-bearing strata from across the Barents Sea and on Svalbard. The association of *Leiosphaeridia, Tasmanites* and *Botryococcus* in the samples from 7121/9-1 point to a high reflux of freshwater and nutrients into the marine Zapffe area and blooming of opportunistic algae species during a period of eutrophy, both associated with the backflow of the tsunamis from mainland Norway (Smelror & Dypvik, 2006). Leiospheres are present deeper in the Hekkingen formation in 7121/9-1 (samples from 2191 and 2205 m MD) and are generally common in the lowermost Hekkingen formation, but they are nowhere as abundant as in the draping black shale samples and so not likely to just originate from Hekkingen formation reworking.

The potential altered glass clasts found in the 2027 m MD SWC, at the transition between the draping black shale and the lowermost Knurr Formation, could be volcanic or impact derived and should be further examined. Volcanic activity associated with the High Arctic Large Igneous Province (HALIP) occurred from the Barremian (130–80 Ma, Polteau et al., 2016, Smelror & Petrov, 2018) and thus postdates both Zapffe and the overlying lower Knurr Formation. Consequently, there is a possibility that the clasts could originate from the Mjølnir ejecta blanket. The sample material has been examined for other mineralogical impact indicators, for example, shocked quartz but so far with no positive results (H. Dypvik, pers.com.). Glauconite is found in abundance in the Myklegardfjellet Bed of the Rurikfjellet Formation on Spitsbergen and could here be ascribed to comparable stratigraphic formations (Dypvik et al., 1992). If the draping black shale interval indeed records the immediate aftermath of the Mjølnir impact, it accurately dates the Zapffe slump itself to the Mjølnir impact time at the Volgian–Ryazanian boundary.

6 | DEPOSITIONAL MODEL FOR THE ZAPPFE UNIT

We interpret the Zapffe slump to represent a single seismogenic event, triggered by the Mjølnir impact (Figure 11). The forcing of the impact earthquake, and

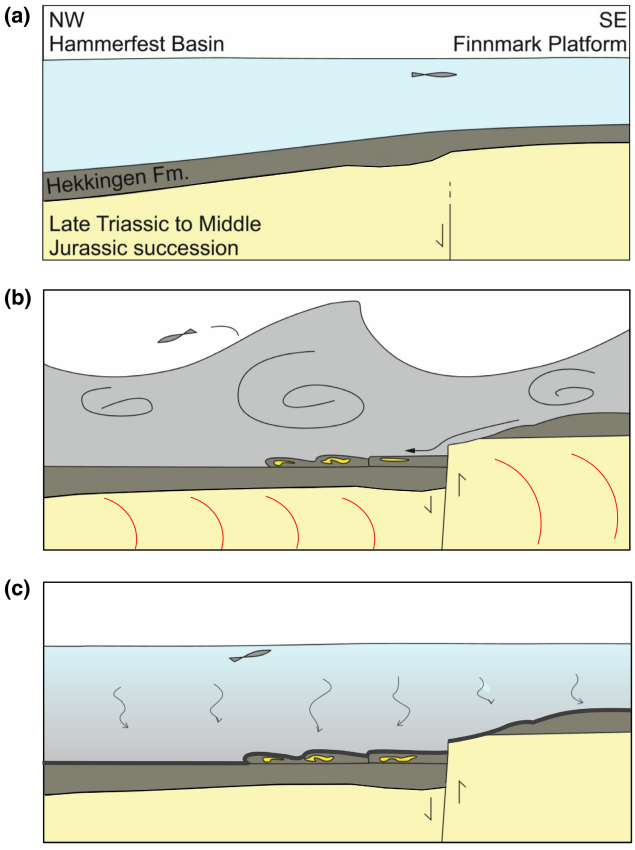

FIGURE 11 Model for formation of the Zapffe slump and draping shale interval, not to scale. (a) Pre-Mjølnir depositional setting of the Hekkingen Formation. The fault segment of the Troms-Finnmark Fault Complex up-dip from the Zapffe unit location has not penetrated to surface and is expressed by a subtle monocline at seabed and a possible shallow depocenter. (b) The shock waves caused by the Mjølnir earthquake, and passage of tsunami trains and associated bottom currents forces the fault to surface and causes a significant offset. Poorly consolidated Hekkingen and Middle Jurassic sand-rich lithologies collapses along the fault scarp and on top of the footwall block and slumps into the basin. The Mjølnir tsunami re-suspends large amounts of Hekkingen Formation mudstone. (c) In immediate post-Mjølnir times the draping black shale is formed by re-settling of suspended Hekkingen Formation mudstone mixed with ejecta from the Mjølnir impact site and opportunistic palynomorph assemblages, the latter fed by nutrients brought into the marine realm from tsunami backwash.

potentially also the associated tsunamis, caused existing but soft-linked faults segments to the east and west of the Zapffe unit to hard-link and propagate to surface. This resulted in the formation of a fault scarp with a significant offset at seabed up-dip from the Zapffe unit (Figure 11b). It is envisaged that the poorly consolidated, clay-dominated lithologies of the Hekkingen and Fuglen formations and underlying Early–Middle Jurassic sand-rich formations collapsed along the thus abruptly exposed high-relief fault scarp. This may have

triggered the large submarine landslide, which travelled into the Hammerfest Basin as a cohesive density flow and was deposited as the Zapffe slump (Figure 11b). The far-field propagation of the impact stress waves through the thick sedimentary succession of the Bjarmeland Platform is not well understood. However, impact generated seismicity has been explored more generally in e.g., Güldemeister and Wünnemann (2017). We consider that the impact shockwaves were several magnitudes larger than those of any recorded earthquakes (Shuvalov et al., 2002). This, in combination with the cyclical stress associated with the passage of trains of giant tsunamis and derived currents may have caused widespread rupture and re-activation of the existing faults. The deep-seated and basement-cored Troms-Finnmark Fault Complex is oriented at a high angle to the shock propagation front in the study area, exposing it to the full effect of the shock waves.

The offset on faults up-dip of the Zapffe unit at the time of the slumping event can be estimated by the dimensions of the inferred outrunner clasts at the frontal part of the slump (but not penetrated by well 7121/9-1), and the origin of the coarse clastic material. Outrunner clasts are generated as blocks avalanching from a cliff face and these can be no taller than the height of the cliff itself, hence their size of 60–100 m indicates a minimum escarpment height. When it comes to the coarse clastic content of the slump observed in well 7121/9-1, this is likely reworked from the fault scarp itself. If the original thickness of the Hekkingen Formation in the footwall of the Troms-Finnmark Fault Complex was similar to that recorded in the 7121/9-1 well, i.e., 200 m, then the offset along the fault segment up-dip of the well would need to have been in the order of 200 m or more to expose pre-Hekkingen lithologies for incorporation into the slump. Alternatively, the coarse clastic content could have been brought into the 7121/9-1 area by backwash from river mouths located up-dip of the Zapffe unit on the Finnmark Platform. Such reflux deposits are commonly observed from modern tsunamis (Bourgeois, 2009), however, our paleoenvironmental interpretation of the upper Hekkingen Formation and foraminiferal assemblages in the Zapffe unit indicates a considerable distance to the coastline on the Finnmark Platform at the time of slumping.

The thickness of the draping black shale; 9 m in well 7121/9-1, might suggest that pre-impact Hekkingen Formation depositional conditions persisted for some time after impact, but with intensified oxygen depletion created by increased nitrification, as would be in general trend with observations from shallow cores adjacent to the crater (Dypvik et al., 2004, 2010). However, we also consider that the draping black shale may be entirely a fallout layer representing re-settling of the large volumes of Hekkingen mud eroded by the Mjølnir tsunami trains (Figure 11c). Significant tsunami erosion of the seabed is suggested by the common presence of an unconformity and associated hiatus between the Hekkingen and Knurr formations immediately north of the Zapffe unit termination. Marin et al. (2021) reports of offshore incisions and potential clinoforms/sediment waves at the same stratigraphic level from several Hammerfest Basin locations (their Figure 11), similar features attributed to the Chicxulub tsunami have been observed in Louisiana (Kinsland et al., 2021). The Hekkingen-Knurr Formation unconformity is recognized across the greater Barents Sea region (Bugge et al., 2002; Marin et al., 2021; Smelror, 2021; Smelror et al., 2001; Wierzbowski & Smelror, 2020), indicating the scale of erosion in the marine basins by the Mjølnir tsunamis setting up bottom current velocities of 30–90 km/h during passage of the wave trains (Glimsdal et al., 2007, 2010). The draping shale interval may therefore record resettling of material over a much shorter time interval than otherwise expected from average Hekkingen accumulation rates of 0.3–0.8 cm/1000 years in the Early and Mid Volgian (cf. Langrock & Stein, 2004).

7 | REGIONAL DISTRIBUTION AND PRESERVATION POTENTIAL OF IMPACT-RELATED DEPOSITIONAL FEATURES

The apparent scarcity of Mjølnir impact-related deposits in the greater Barents Sea and Northeast Greenland is puzzling, considering the modelled magnitude of the Mjølnir-generated earthquake and associated bottom currents and tsunami trains. For other documented marine impacts, there is a growing portfolio of studies documenting widespread shelf collapse along the basin margins and tsunami-related deposits from basin floor to the coastal plain regions.

The Chicxulub asteroid, which created a 200 km-in-diameter crater on the Yucatán peninsula at the Cretaceous- Paleogene boundary, triggered collapse of parts of the continental margin around the Gulf of Mexico, and slumping of shallow marine deposits to the deep sea along the eastern margin of North America (Bralower et al., 1998, 2010; Goto et al., 2008; Norris & Firth, 2002; Sanford et al., 2016; Scott et al., 2014). The impact-triggered currents/tsunamis radiated across the Gulf of Mexico, crashing onto nearby coastlines, but also farther across the proto-Caribbean and Atlantic basins (e.g., Gulick et al., 2019; Kring, 2007; Sanford et al., 2016; Smit, 1999). The impact-triggered tsunamis may have

penetrated more than 300 km inland (DePalma et al., 2019; Matsui et al., 2002), and major volumes of sediments derived from coastal and shallow-water environments was redeposited via seismic and mega-tsunamic processes (Kinsland et al., 2021; Sanford et al., 2016; Whalen et al., 2020).

Although the Chicxulub asteroid was an order of magnitude larger than Mjølnir, the depositional response to the impact perturbations could have been of a similar nature. The expected response of the local depositional environments to the Mjølnir impact and the preservation potential of impact-related deposits should therefore be viewed in the context of the tectonic and palaeogeographical setting. The study area for this paper was located offshore, in a distal prodelta setting prior to the Mjølnir event. The Zapffe slump and the draping black shale, thus deposited offshore in the newly formed hangingwall of a major fault, had a high potential of preservation from subsequent reworking due to its location in the basin. However, slumped deposits are a common constituent of marine syn-rift fault aprons and correct association of such deposits with an impact requires the presence and recognition of a unique time-marker—for example, a layer containing impact related biostratigraphic or chemical components.

Chicxulub impact ejecta are found globally in continental and marine deposits (Schulte et al., 2010; Smit, 1999), indicating that unique time-marker layers should be recognizable given they are preserved. The Chesapeake Bay impact caused a sharp decline in microfossil abundances, suggesting the regional adverse effects on fauna and flora caused by the impact, and traces of ejecta have been found in sediments along the East Coast of US, about 330 km away (Glass et al., 1998). For Mjølnir, these components are documented across the Barents Sea region from Svalbard to Sibir. The black draping shale, the unique time marker for the Zapffe slump, is most likely limited to no more than a few metres thickness in the Hammerfest Basin. Most hydrocarbon exploration wells in the Barents Sea have targeted Lower Jurassic reservoirs and the biostratigraphic material available for dating of the Mjølnir time-equivalent overburden section therefore typically consist of ditch cuttings with 10–30 m sampling intervals. Consequently, a thin layer like this may easily be missed purely due to undersampling.

Late Jurassic–Early Cretaceous nearshore successions are preserved in Northeast Greenland (Dypvik et al., 2002; Håkansson et al., 1981). The Loppa High was likely also emergent at Jurassic—Cretaceous boundary time and nearshore deposits are expected to have existed along the eastern margin of this high (Marin et al., 2018, 2021). We consider it likely that the Mjølnir impact triggered widespread collapse of coastal sediment accumulations and tsunami-related erosion of the coastal plains as also observed from the Chicxulub impact (Norris & Firth, 2002; Scott et al., 2014). Attempts to identify effects of the Mjølnir impact in nearshore successions in Northeast Greenland have so far been unsuccessful (Dypvik et al., 1998). We speculate, though, that the undated, lowermost part of the Knurr Formation sandstone wedge at the Southeast margin of the Loppa High, penetrated by well 7122/2-1 may be related to delta collapse and/or tsunami backflow from a river system draining the eastern flank of the high. This wedge erosively overlies Oxfordian Hekkingen formation mudstones and is in turn overlain by Early Cretaceous mudstones. The lowermost 20 m of the cored section (1920–1931.8 m MD) of the Knurr Formation consist of massive density flow deposits with a clast assemblage of pedogenically altered mudstones from a floodplain and light bioturbated mudstones likely representing the Late Jurassic proximal shelf. The overlying part of the Knurr Formation in this well has a well-established Valanginian age, which suggests that any Mjølnir-related deposits along the more proximal Loppa High margin were removed during subsequent Early Cretaceous lowstands (Marin et al., 2018). A possible analogue from the Chesapeake Bay impact basin is presented by Schulte et al. (2009) who remarked that appearance of coarse clastic sediments in the offshore environment across the Eocene—Oligocene boundary, could be related to erosion, winnowing, and reworking of deposits originally related to the Late Eocene Chesapeake Bay Impact. This highlights that the preservation potential of earthquake and tsunami effects in nearshore environments are much lower than in the deep parts of a basin, due to fluvial and coastal reworking processes.

The understanding of tectonic and depositional responses to the perturbations of marine impacts is still growing, as is the understanding of the significance of the tectonic grain and palaeogeography for the nature and preservation potential of impact-related deposits. Considerations for the expected impact perturbations and their likely effect in various parts of the depositional basin may lead to a better understanding of where and how impact deposits may have formed, where they may be preserved today and thus where to explore for them in the future.

8 | CONCLUSIONS

The Zapffe unit is a large slump deposit located in the hanging-wall of the Troms-Finnmark Fault Complex and penetrated by well 7121/9-1. It is time-wise accurately attributed to the Mjølnir impact by a black shale draping the slump, which contains a conspicuous palynomorph assemblage known from immediate post impact strata across the Barents Sea.

The Zapffe unit sharply overlies Hekkingen formation marine mudstones and marks the sudden generation of significant topography along the Troms-Finnmark Fault Complex up-dip to the south. The implication of its morphology, lithological content and stratigraphic context is that the Mjølnir impact likely triggered the linkage and emergence of fault segments in the fault zone and created a submarine cliff that was at least 60 m and potentially more than 200 m high immediately up-dip of the Zapffe unit.

The draping black shale records the immediate post-impact ecological crisis caused by tsunami backwash of freshwater and nutrients into the marine realm. This several-meter thick interval may represent re-settling of large volumes of Hekkingen formation mud, eroded from the seabed across the Hammerfest basin by wave motion and bottom currents set up by the Mjølnir tsunami trains.

The preservation potential for this type of impact deposits is high in the offshore part of a basin. Such deposits are, however, easy to overlook since the depositional processes implied are non-unique to impacts. Certain recognition depends on precise dating by means of a biostratigraphic or geochemical fingerprints, as is here the case of the draping black shale here.

We speculate that other Mjølnir impact deposits are preserved in the Barents Sea and surrounding basins but may have been overlooked due to a combination of poor dating and lack of observance of the link between palaeogeography and Mjølnir impact-generated physical processes.

ACKNOWLEDGEMENTS

Thanks to PGNiG Upstream Norway AS (formerly DONG E&P Norwa AS) for providing access to various proprietary reports and seismic data related to the 7121/9-1 well. The manuscript has benefited greatly from constructive comments and suggestions from reviewers Auriol Rae, Uisdean Nicholson and Sean Gulick.

FUNDING INFORMATION

The authors received no funding for this article.

PEER REVIEW

The peer review history for this article is available at https://publons.com/publon/10.1111/bre.12725.

DATA AVAILABILITY STATEMENT

Original seismic and well data that support the findings of this study is the property of DONG E&P AS, now PGNiG Upstream Norway AS. The raw data are publicly available through the Norwegian DISKOS National Data Repository, whereas some of the derived data (non-public reports on petrography and biostratigraphy relating to well 7121/9-1) is the property of PGNiG Upstream Norway and may be obtained by permission from the owner. Biostratigraphic analysis data conducted for this study can be made available by contacting the authors.

ORCID

Rikke Bruhn https://orcid.org/0000-0002-6166-4586

REFERENCES

Azbel, A.J. & Grigyalis, A.A. (1991). *Practical advisory in the micropaleontology of the SSSR. Vol. 5. Mesozoic foraminifera*. Vsesoyuznyy Nauchno-Issledovateskiy Geologorazvedochnyy Institut (VNIGRI), pp. 1–375 (in Russian).

Basov, V. A., Vasilenko, L. V., Sokilov, A. O., & Yakovleva, S. P. (1989). Zonal subdivision of Mesozoic deposits of the Barents Basin. In *Stage and zonal scale of the Boreal Mesozoic in the SSSR* (Vol. *722*, pp. 60–73). Institut Geologii i Geofiziki Sibirskoe Otdelenie, Akademiya Nauk SSSR (in Russian).

Bjærke, T. (1980). Mesozoic palynology of Svalbard V. – Dinoflagellates from the Agardhfjellet member (middle and upper Jurassic) in Spitsbergen. *Norsk Polarinstitut Skrifter*, *172*, 145–168.

Bourgeois, J. (2009). Geological effects and records of tsunamis. In A. R. Robinson & E. N. Bernard (Eds.), *Tsunamis* (pp. 53–91). Harvard University Press.

Bralower, T., Eccles, L., Kutz, J., Yancey, T., Schueth, J., Arthur, M., & Bice, D. (2010). Grain size of Cretaceous-Paleogene boundary sediments from Chicxulub to the open ocean: Implications for interpretation of the mass extinction event. *Geology*, *38*, 199–202.

Bralower, T. J., Paull, C. K., & Leckie, R. M. (1998). The Cretaceous-tertiary boundary cocktail: Chicxulub impact triggers margin collapse and extensive sediment gravity flows. *Geology*, *26*, 331–334.

Bremer, G. M. A., Smelror, M., Nagy, J., & Vigran, J. O. (2004). Biotic responses to the Mjølnir meteorite impact, Barents Sea: Evidence from a Core drilled within the crater. In H. Dypvik, M. J. Burchell, & P. Claeys (Eds.), *Cratering in marine environments and on ice. Impact studies* (pp. 21–38). Springer.

Bugge, T., Elvebakk, G., Fanavoll, S., Mangerud, G., Smelror, M., Weiss, H., Gjelberg, J., Kristensen, S. E., & Nilsen, K. (2002). Shallow drilling applied to hydrocarbon exploration of the Nordkapp Basin, Barents Sea. *Marine and Petroleum Geology*, *19*, 13–37.

Bulynnikova, S. P., Komissarenko, V. K., Belousova, N. A., Bogomjakova, E. D., Rylkova, G. E., & Tylkina, K. E. (1990). *Atlas of mollusca and foraminifera from Upper Jurassic and Neocomian marine deposits of the Western Siberian oil bearing area. Vol. 2. Foraminifera* (pp. 1–395). Sibirskiy Nauchno-issledovatelskiy Institut Geologii, Geofiziki i Mineralnogo Syrya (SNIIGGIMS) (in Russian).

Burfoot, W. & Dunk, A. (2012). *Geological & routine core analysis investigation of nine sidewall core samples from well 7121/9-1 (Zapffe field)*. Core Lab report RES GEO 120107 for Dong Energy E&P Norge AS. Unpublished.

Costa, L. I., & Davey, R. J. (1992). Dinoflagellate cysts of the Cretaceous system. In A. J. Powell (Ed.), *A stratigraphic index of dinoflagellate cysts. British Micropalaeontological society publication series* (pp. 99–153). Chapman & Hall.

DePalma, R., Smit, J., Brunham, D. A., Kuiper, K., Manning, P. L., Oleinik, A., Larson, P., Maurrasse, F. J., Vellekoop, J., Richards, M. A., Gurche, L., & Alvarez, W. (2019). A seismically induced onshore surge deposit at the KPg boundary, North Dakota. *Proceedings of the National Academy of Sciences of the United States of America*, *116*, 8190–8199.

Dypvik, H., & Attrep, M. (1999). Geochemical signals of the Late Jurassic, marine Mjølnir impact. *Meteoritics and Planetary Science*, *34*, 393–406.

Dypvik, H., & Ferrell, R. E. (1998). Clay mineral alteration associated with a meteorite impact in the marine environment (Barents Sea). *Clay Minerals*, *33*, 51–64.

Dypvik, H., Gohn, G. S., Edwards, L. E., Horton, J. W., Powars, D. S., & Litwin, R. S. (2018). Chesapeake Bay impact structure – Development of «brim» sedimentation in a multilayered marine target. *Geological Society of America, Special Paper*, *537*, 68.

Dypvik, H., Gudlaugsson, S. T., Tsikalas, F., Attrep, M., Ferrell, R. E., Kringsley, D. H., Mørk, A., Faleide, J. I., & Nagy, J. (1996). Mjølnir structure: An impact crater in the Barents Sea. *Geology*, *24*, 779–782.

Dypvik, H., Håkansson, E., & Heinberg, C. (2002). Jurassic and Cretaceous palaeogeography and stratigraphiv comparisons in the North Greenland-Svalbard region. *Polar Research*, *21*, 91–108.

Dypvik, H., Håkansson, E., Heinberg, C., & Bruhn, R. (1998). *Geologisk Feltarbeid på Nordgrønland 1998*. Unpublished field report for Norsk Hydro, Saga Petroleum and the University of Copenhagen.

Dypvik, H., Mørk, A., Smelror, M., Sandbakken, P. T., Tsikalas, F., Vigran, J. O., Bremer, G. M. A., Nagy, J., Gabrielsen, R., Faleide, J. I., Bahiru, G. M., & Weiss, H. M. (2004). Impact breccia and ejecta from the Mjølnir crater in the Barents Sea – The Ragnarok formation and the Sindre bed. *Norwegian Journal of Geology*, *84*, 143–167.

Dypvik, H., Nagy, J., & Krinsley, D. H. (1992). Origin of the Myklegardfjellet bed, a basal Cretaceous marker in Svalbard. *Polar Research*, *10*, 21–31.

Dypvik, H., Tsikalas, F., & Smelror, M. (Eds.). (2010). *The Mjølnir impact event and its consequences: Geology and geophysics of a Late Jurassic/Early Cretaceous marine impact event* (p. 318). Springer Verlag.

Faleide, J. I., Bjørlykke, K., & Gabrielsen, R. H. (2015). Geology of the Norwegian continental shelf. In K. Bjørlykke (Ed.), *Petroleum geoscience*. Springer, Berlin.

Fenton, J., Hawkes, J., Henderson, A., Enichetti, E., Mullins, G. & Rich, B. (2012). 7121/9-1 (Zapffe) biostratigraphy. Robertson report No. 7165/Ia for Dong E&P Norge AS. Unpublished.

Gabrielsen, R. (1984). Long-lived fault zones and their influence on the tectonic development of the southwestern Barents Sea. *Journal of the Geological Society*, *141*, 651–662.

Gabrielsen, R. H., Færseth, R. B., Jensen, L. N., Kalheim, J. E., & Riis, F. (1990). Structural elements of the Norwegian continental shelf. Part 1: The Barents Sea region. *Norwegian Petroleum Directorate Bull*, *6*, 33.

Georgiev, S., Stein, H., Hannah, J. L., Xu, G., Bingen, B., & Weiss, H. M. (2017). Timing, duration, and causes for Late Jurassic–Early Cretaceous anoxia in the Barents Sea. *Earth and Planetary Science Letters*, *461*, 151–162.

Glass, B. P., Koeberl, C., Blum, J. D., & McHugh, C. M. G. (1998). Upper Eocene tektite and impact ejecta layer on the continental slope off New Jersey. *Meteoritics and Planetary Science*, *33*, 229–241.

Glimsdal, S., Pedersen, G. K., Langtangen, H. P., Shuvalov, V., & Dypvik, H. (2007). Tsunami generation and propagation from the Mjølnir asteroid impact. *Meteoritics and Planetary Science*, *42*, 1473–1493.

Glimsdal, S., Pedersen, G. K., Langtangen, H. P., Shuvalov, V., & Dypvik, H. (2010). The Mjølnir tsunami. In F. Tsikalas, H. Dypvik, & M. Smelror (Eds.), *The Mjølnir impact event and its consequences. Impact studies*. Springer.

Gohn, G. S., Koeberl, C., Miller, K. G., & Reimold, W. U. (2009). The ICDP-USGS deep Drilliong project in the Chesapeake Bay impact structure: Results from the Eyreville Core holes. *Geological Society of America, Special Paper*, *458*, 975.

Gomez, C., Hardouin, D., & Le Ruyet, T. (2012). *Final report for the 3D seismic data processing of PL518/PL229 (DG0901/DG09M01), Offshore Norway. Time and depth processing*. CGGVeritas report 103m9ip/103m9iq for DONG E&P AS. Unpublished.

Goto, K., Ryuji, T., Tajika, E., Iturralde-Vinent, M. A., Takafumi, M., Shinji, Y., Yoichiro, N., Tatsuo, O., Shoichi, K., Delgado, D. E. G., Otero, C. D., & Consuegra, R. R. (2008). Lateral lithological and compositional variations of the Cretaceous/tertiary deep-sea tsunami deposits of northwestern Cuba. *Cretaceous Research*, *29*, 217–236.

Gudlaugsson, S. T. (1993). Large impact crater in the Barents Sea. *Geology*, *21*, 291–294.

Güldemeister, N., & Wünnemann, K. (2017). Quantitative analysis of impact-induced seismic signals by numerical modelling. *Icarus*, *296*, 15–27.

Gulick, S.P.S., Bralower, T.J., Ormö, J., Hall, B., Grice, K., Schaefer, B., Lyons, S., Freeman, K.H., Morgan, J.V., Artemieva, N., Kaskes, P., de Graaf, S.J., Whalen, M.T., Collins, G.S., Tikoo, S.M., Verhagen, C., Christesno, G.L., Claeys, P., Coolen, M.J.L., … Wittmann, A.; Expedition 364 Scientists. (2019). The first day of the Cenozoic. *Proceedings of the National Academy of Sciences*, *116*, 19342–19351.

Gulick, S. P. S., Christeson, G. L., Barton, P. J., Grieve, R. A. J., Morgan, J. V., & Urritia-Fucugauchi, J. (2013). Geophysical characterization of the Chicxulub impact crater. *AGU Revies of Geophysics*, *51*, 31–52.

Håkansson, E., Birkelund, T., Piasecki, S., & Zakharov, V. (1981). Jurassic-Cretaceous boundary strata of the extreme Arctic (Peary Land, North Greenland). *Bulletin of the Geological Society of Denmark*, *30*, 11–42.

Hannah, J. L., Stein, H. J., Goswami, V., & Dypvik, H. (2020). Re-Os chronology of the Mjølnir meteorite crater, Barents Sea: Impact age and seawater recovery, 948. https://doi.org/10.46427/gold2020.948

Hildebrand, A. R., Pilkington, M., Connors, M., Ortiz-Aleman, M., & Chavez, R. E. (1995). Size and structure of the Chicxulub crater revealed by horizontal gravity gradients and cenotes. *Nature*, *376*, 415–417.

Kinsland, G. L., Egedal, K., Strong, M. A., & Ivy, R. (2021). Chicxulub impact tsunami megaripples in the subsurface of Louisiana: Imaged in petroleum industry seismic data. *Earth and Planetary Science Letters*, *570*, 1–9.

Kring, D. A. (2007). The Chicxulub impact event and its environmental consequences at the Cretaceous–tertiary boundary. *Palaeogeography, Palaeoclimatology, Palaeoecology*, *255*, 4–21.

Langrock, U., & Stein, R. (2004). Origin of marine petroleum source rocks from the Late Jurassic to Early Cretaceous Norwegian

Greenland seaway—Evidence for stagnation and upwelling. *Marine and Petroleum Geology*, *21*, 157–176.

Marin, D., Escalona, A., Grundvåg, S.-A., Olaussen, S., Sandvik, S., & Slivinska, K. K. (2018). Unravelling key controls on the rift climax to post-rift fill of marine basins: Insights from the 3D seismic analysis of the lower Cretaceous of the Hammerfest Basin, SW Barents Sea. *Basin Research*, *30*, 587–612.

Marin, D., Helleren, S., Escalona, A., Olaussen, S., Cedeno, A., Nøhr-Hansen, H., & Ohm, S. (2021). The middle Jurassic to lowermost Cretaceous in the SW Barents Sea: Interplay between tectonics, coarse-grained sediment supply and organic matter preservation. *Basin Research*, *33*, 1033–1055.

Matsui, T., Imamura, F., Tajika, E., Nakano, Y., & Fujisawa, Y. (2002). Generation and propagation of a tsunami from the Cretaceous–Tertiary impact event. In C. Koeberl & K. G. MacLeod (Eds.), *Catastrophic events and mass extinctions: Impacts and beyond* (Vol. *356*, pp. 69–77). Geological Society of America, Special Paper.

Morgan, J., Gulick, S., Bralower, T., Chenot, E., Christeson, G., Claeys, P., Cockell, C., Collins, G. S., Coolen, M. J. L., Ferrière, L., Gebhardt, C., Goto, K., Jones, H., Kring, D. A., Le Ber, E., Lofi, J., Long, X., Lowery, C., Mellett, C., … Zylberman, W. (2016). The formation of peak rings in large impact craters. *Science*, *354*(6314), 878–882.

Mørk, A., Dallmann, W., K., Djupvik, H., Johannessen, E. P., Larssen, G. B., Nagy, J., Nøttvedt, A., Olaussen, S., Pčelina, T. M., & Worsley, D. (1999). Mesozoic lithostratigraphy. In: Dallmann, W. K. (Ed.), *Lithostratigraphic lexicon of Svalbard. Review and recommendations for nomenclature use. Upper Palaeozoic to quaternary bedrock*, 127–214. Norsk Polarinstitutt, Tromsø.

Mulrooney, M. J., Leutscher, J., & Braathen, A. (2017). A 3D structural analysis of the Goliat field, Barents Sea, Norway. *Marine and Petroleum Geology*, *86*, 192–212.

Murray, J. W. (2006). *Ecology and applications of benthic foraminifera* (pp. 1–426). Cambridge University Press.

Muzaffar, W. (2018). *A detailed structural investigation of the Alke structure, SW Hammerfest Basin - Geometry, timing and genesis* (p. 101). Master Thesis from the University of Oslo.

Nagy, J. (2005). Delta-influenced foraminiferal facies and sequence stratigraphy of Paleocene deposits in Spitsbergen. *Palaeogeography, Palaeoclimatology, Palaeoecology*, *222*, 161–179.

Nagy, J., & Basov, V. A. (1998). Revised foraminiferal taxa and biostratigraphy of Bathonian to Ryazanian deposits in Spitsbergen. *Micropaleontology*, *44*, 217–255.

Nagy, J., Hess, S., & Alve, E. (2010). Environmental significance of foraminiferal assemblages dominated by small-sized Ammodiscus and Trochammina in Triassic and Jurassic delta influenced deposits. *Earth-Science Reviews*, *99*, 31–49.

Norris, R. D., & Firth, J. V. (2002). Mass wasting of Atlantic continental margins following the Chicxulub impact event. *Geological Society of America, Special Paper*, *356*, 79–95.

Nyjordet, B., Urdal, K., Harding, R., Johansen, I. & Hansen, G. (2012). *Geochemistry Data Report – Well 7121/9-1 (Zapffe)*. Applied Petroleum Technology, report APT12-2887 for Dong E&P AS. Unpublished.

Polteau, S., Hendriks, B. W., Planke, S., Ganerød, M., Corfu, F., Faleide, J. I., Midtkandal, I., Svendsen, H. S., & Myklebust, R. (2016). The Early Cretaceous Barents Sea Sill Complex: Distribution, 40Ar/39Ar geochronology, and implications for carbon gas formation. *Palaeogeography, Palaeoclimatology, Palaeoecology*, *441*, 83–95.

Poulsen, N. E., & Riding, J. B. (2003). The Jurassic dinoflagellate cyst zonation of subboreal Northwest Europe. *Geological Survey of Denmark and Greenland Bulletin*, *1*, 115–144.

Powars, D. S., Poag, C. W., & Mixon, R. B. (1993). The Chesapeake bay "impact crater"; stratigraphic and seismic evidence. *Geological Society of America Abstracts with Programs*, *25*, 378.

Reolid, M., Nikitenko, B. L., & Glinskikh, L. (2014). Trochammina as opportunist foraminifera in the lower Jurassic from North Siberia. *Polar Research*, *33*, 1–13.

Riding, J. B., & Thomas, J. E. (1992). Dinoflagellate cysts of the Jurassic system. In A. J. Powell (Ed.), *A stratigraphic index of dinoflagellate cysts. British Micropalaeontological Society Publication Series* (pp. 7–97). Chapman & Hall.

Rokoengen, K., Mørk, A., Mørk, M. B. E., & Smelror, M. (2005). The irregular base Cretaceous reflector offshore mid Norway: A possible result of the Mjølnir impact in the Barents Sea? *Norwegian Geological Survey Bulletin*, *443*, 19–27.

Sanford, J. C., Snedden, J. W., & Gulick, S. P. (2016). The Cretaceous-Paleogene boundary deposit in the Gulf of Mexico: Large-scale oceanic basin response to the Chicxulub impact. *Journal of Geophysical Research - Solid Earth*, *121*, 1240–1261.

Schulte, P., Wade, B. S., Kontny, A., & Self-Trail, J. M. (2009). The Eocene – Oligocene sedimentary record in the Chesapeake Bay impact structure: Implication for climate and sea-level changes on the western Atlantic margin. *The Geological Society of America, Special Paper*, *458*, 839–867.

Schulte, P., Alegret, L., Arenillas, I., Arz, J. A., Barton, P. J., Bown, P. R., Bralower, T. J., Christeson, G. L., Claeys, P., Cockell, C. S., Collins, G. S., Deutsch, A., Goldin, T. J., Goto, K., Grajales-Nishimura, J. M., Grieve, R. A. F., Gulick, S. P. S., Johnson, K. R., Kiessling, W., … Willumsen, P. S. (2010). The Chicxulub asteroid impact ejecta and mass extinction at the Cretaceous – Palaeogene boundary. *Science*, *327*, 1214–1218.

Scott, E. D., Denne, R. A., Kaiser, J. S., & Eickhoff, D. P. (2014). Impact on sedimentation into the north-Central Deepwater Gulf of Mexico as a result of the Chicxulub event. *Journal of the Gulf Coast Association of Geological Societies*, *3*, 41–50.

Shuvalov, V., Dypvik, H., & Tsikalas, F. (2002). Numerical simulations of the Mjølnir marine impact crater. *Journal of Geophysical Research*, *107*, 1–13.

Smelror, M. (2021). Palynostratigraphy, palynofacies, T-R cycles and paleoenvironments in the middle Jurassic-Early Cretaceous Ramså Basin, Andøya, northern Norway. *Geosciences*, *11*, 32.

Smelror, M., & Dypvik, H. (2005). Marine microplankton biostratigraphy of the Volgian-Ryazanian boundary strata, western Barents shelf. *NGU Bulletin*, *442*, 61–69.

Smelror, M., & Dypvik, H. (2006). The sweet aftermath: Environmental changes and biotic restoration following the marine Mjølnir impact (Volgian – Ryazanian boundary, Barents shelf). In *Biologic processes associated with impacts* (pp. 143–178). Springer Verlag.

Smelror, M., Dypvik, H., & Mørk, A. (2002). Phytoplankton blooms in the Jurassic Cretaceous boundary beds of the Barents Sea possibly induced by the Mjølnir impact. In E. Buffetaut & C. Koeberl (Eds.), *Geological and biological effects of impact events. Lecture notes in earth sciences, impact studies* (pp. 69–81). Springer.

Smelror, M., Kelly, S. R. A., Dypvik, H., Mørk, A., Nagy, J., & Tsikalas, F. (2001). Mjølnir (Barents Sea) meteorite impact offers a Volgian-Ryazanian boundary marker. *Newsletter on Stratigraphy*, *38*, 129–140.

Smelror, M., & Petrov, O. V. (2018). Geodynamics of the Arctic: From Proterozoic orogens to present day seafloor spreading. *Journal of Geodynamics*, *121*, 185–204.

Smit, J. (1999). The global stratigraphy of the Cretaceous–tertiary boundary impact ejecta. *Annual Review of Earth and Planetary Sciences*, *27*, 75–113.

Tsikalas, F., Gudlaugsson, S. T., Eldholm, O., & Faleide, J. I. (1998). Integrated geophysical analysis supporting the impact origin of the Mjølnir structure, Barents Sea. *Tectonophysics*, *239*, 257–280.

Whalen, M.T., Gulick, S.P.S., Lowery, C.M., Bralower, T.J., Morgan, J.V., Grice, K., Schaefer, B., Smit, J., Ormö, J., Wittmann A., Kring, D.A., Lyons, S., Goderis S., & the IODP-ICDP Expedition 364 Scientists. (2020). Winding down the Chicxulub impact: The transition between impact and normal marine sedimentation near ground zero, *Marine Geology*, *430*, 106368.

Wierzbowski, A., & Smelror, M. (2020). The Bajocian to Kimmeridgian (middle to upper Jurassic) ammonite succession at Sentralbanken (core 7533/7-U-1), Barents Sea, and its stratigraphical and palaeogeographical significance. *Volumina Jurassica*, *18*, 1–22.

Worsley, D., Johansen, R., & Kristensen, S. E. (1988). The Mesozoic and Cenozoic succession of Tromsøflaket. In A. Dalland, D. Worsley, & K. Ofstad (Eds.), *A lithostratigraphic scheme for the Mesozoic and Cenozoic succession offshore mid and northern Norway. NPD Bulletin No. 4* (p. 65). Norwegian Petroleum Directorate.

Zakharov, V. A., Laphukov, A. S., & Shenfil, O. V. (1993). Iridium anomaly at the Jurassic-Cretaceous boundary in northern Siberia. *Russian Journal of Geology and Geophysics*, *34*, 83–90.

How to cite this article: Bruhn, R., Nagy, J., Smelror, M., Dypvik, H., Glimsdal, S., Pegrum, R., & Cavalli, C. (2022). Shaking and splashing—A case study of far-field effects of the Mjølnir asteroid impact on depositional environments in the Barents Sea. *Basin Research*, *00*, 1–22. https://doi.org/10.1111/bre.12725

APPENDIX A

Palynomorphs and visual kerogen from the Zapffe unit in well 7121/9-1. Depth in meter MD. (1) *Circulodinium distinctum* Jansonius 1986 (DC sample 2020). (2–3) *Tasmanites* sp. (SWC sample 2031). (4) Amorphous organic matter, dark coaly fragment and juvenile *Botryococcus* sp. (SWC sample 2031). (5) Amorphous organic matter (SWC sample 2031).

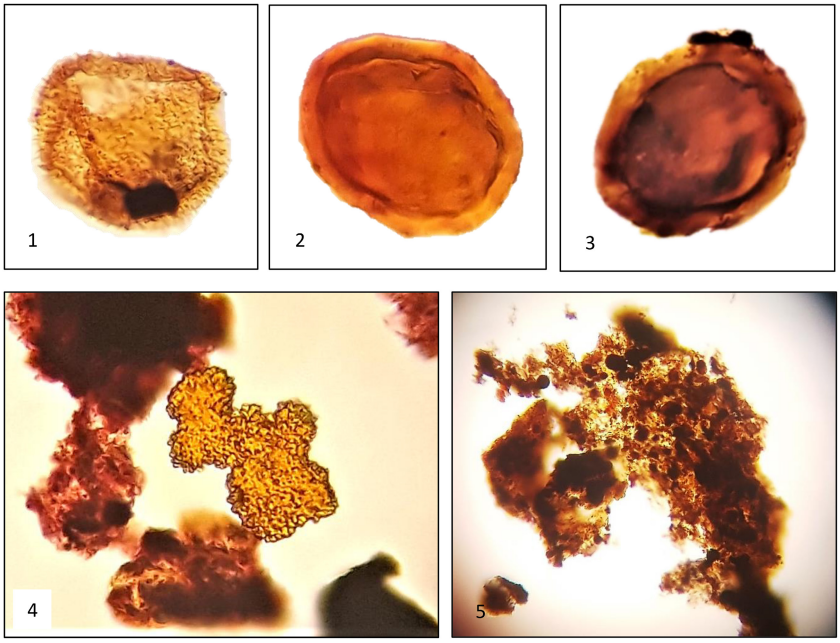

APPENDIX B

Dinoflagellate cysts from the Zapffe unit in well 7121/9-1. Depth in meter MD. (1) *Systematophora daveyi* Riding & Thomas 1988 (DC sample 2020 m). (2) *Rhynchodiniopsis martonensis* Bailey et al. 1997 (DC sample 2020 m). (3) Tubotuberella apatela (Cookson & Eisenack) Ioannides et al. 1977 (DC sample 2020 m). (4) *Systematophora daveyi* Riding & Thomas 1988 (SWC sample 2058 m). (5–6) *Gochteodinia villosa* (Vozzhennikova) Norris 1978 (DC sample 2020 m). (7) *Egmontodinium* sp. (DC sample 2074). (8) *Egmontodinium expiratum* Davey 1982 (DC sample 2074). (9) *Atopodinium haromense* Thomas & Cox 1988 (DC sample 2020 m).

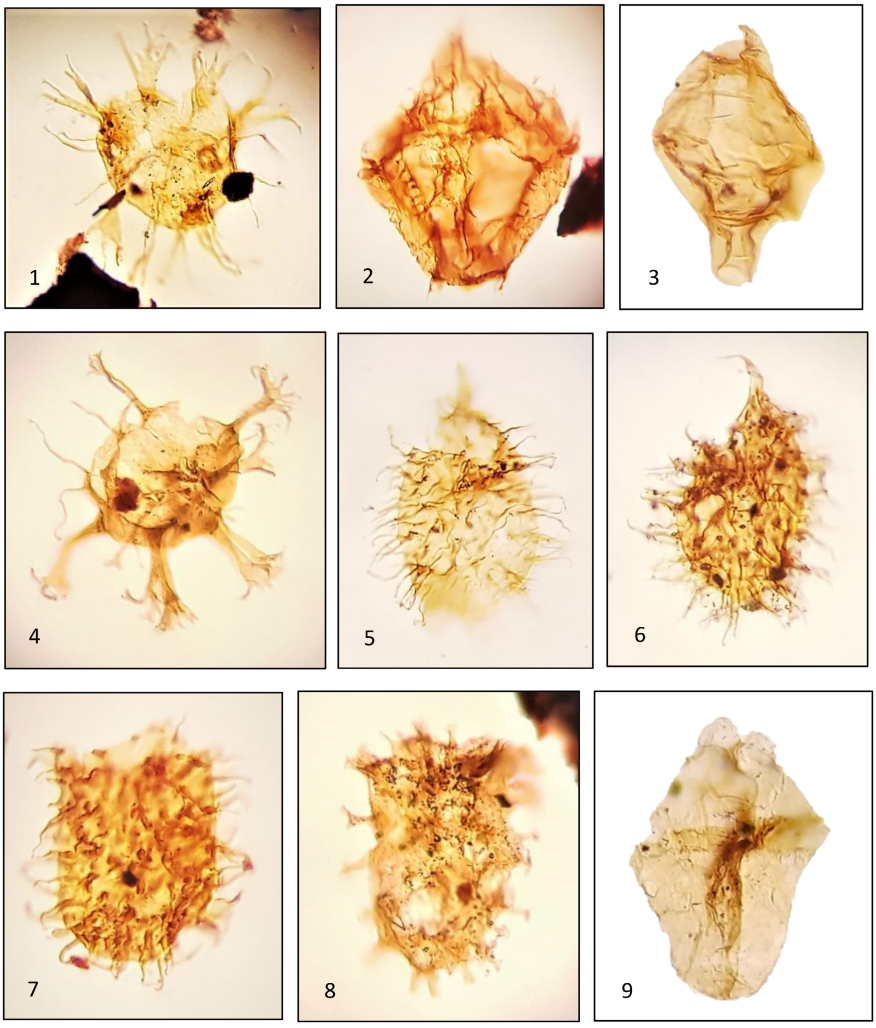

APPENDIX C

Foraminiferal species from the lower and middle part of the Zapffe unit in well 7121/9-1. All photographs ate taken in semi transmitted light except no 20, which is taken in reflected light. Depth in meter MD. (1–2) *Saccammina orbiculata* Bulatova 1964: no 1, 2065 m; no 2, 2062. (3) *Thurammina papillata* Brady 1879: 2074 m. (4) *Glomospira* aff. *Oxfordiana* Scharovskaja 1966: 2062 m. (5) *Saccammina inanis* Gerke et Sossipatrova 1961: 2071 m. (6) *Kutsevella difficilis* (Kusina) 1964: 2074 m. (7) *Recurvoides transitorius* Bulynnikova 1973: 2062 m. (8) *Recurvoides praeobskiensis* Dain et Bulynnikova 1985: 2059 m. (9) *Ammodiscus micrus* Rylkova 1979: 2062 m. (10) *Recurvoides paucus* Dubrovskaja 1962: 2059 m. (11–12) *Trochammina rosacea* Zaspelova 1948: no 11, 2062 m; no 12, 2074 m. (13–14) *Trochammina* annae Levina 1972: no 13, 2071 m; no 14, 2062 m. (15) *Spiroplectammina improcera* Bulynnikova 1990: 2071 m. (16–17) *Verneuilinoides postgraciosus* Komissarenko 1972: no 16, 2071 m; no 17, 2068 m. (18–19) *Dorothia tortuosa* Dain et Komissarenko 1972: no 18, 2062 m; no 19, 2062 m. (20) *Eomarssonella* sp. 2071 m. (21) *Lenticulina* aff. *gigantella* Romanova 1960: 2065 m. (22) *Lenticulina pseudoarctica* Ivanova 1970: 2059 m. (23) *Lenticulina* aff. *parahybrida* Dain 1972: 2071 m.